Journal of Nanobiotechnology

RESEARCH

Open Access

Ligustrazine nano-drug delivery system ameliorates doxorubicin-mediated myocardial injury via piezo-type mechanosensitive ion channel component 1-prohibitin 2-mediated mitochondrial quality surveillance

Junyan Wang[1], Haowen Zhuang[1], Chun Li[1], Ruiqi Cai[2], Hongshuo Shi[3], Boxian Pang[4], Zhijiang Guo[5], Sang-Bing Ong[5], Yifeng Nie[4*], Yingzhen Du[6*], Hao Zhou[7*] and Xing Chang[8*]

Abstract

Background Doxorubicin (DOX) demonstrates significant therapeutic and anticancer efficacy. Nevertheless, it demonstrates significant cardiotoxicity, resulting in permanent cardiac damage. Ligustrazine (LIG) is a bioactive alkaloid derived from the rhizome of the medicinal plant Ligusticum chuanxiong Hort. The alkaloid has exhibited cardioprotective properties. The therapeutic application of LIG is constrained by inadequate water solubility, fast breakdown, and low bioavailability. Nanoparticle drug delivery technologies effectively address these constraints by encapsulating LIG into nanocarriers, significantly enhancing its solubility and bioavailability, hence maximizing its therapeutic efficacy. Consequently, this study employed tetrahedral backbone nucleic acid molecules as LIG carriers. Furthermore, animal models and single-cell sequencing analyses were employed to forecast the mechanisms and targets of pertinent studies. A mouse model genetically modified for the piezo type mechanosensitive ion channel component 1 (PIEZO1), transmembrane BAX inhibitor motif containing 6 (TMBIM6), and prohibitin 2 (PHB2), along with an in vivo and in vitro model of DOX-induced cardiomyopathy (DIC), was established, and a gene-modified cellular system comprising upstream genes and downstream effector targets was constructed. The mechanism of LIG was validated by molecular biology and integrated pharmacology with the implementation of the LIG nano-drug loading method.

Results LIG nano-delivery enhanced DOX-induced cardiac dysfunction and mitochondrial impairment by modulating the PHB2Ser91/Ser176 phosphorylation axis through PIEZO1-TMBIM6, and significantly suppressed cardiomyocyte pyroptosis resulting from mitochondrial homeostasis dysregulation. The findings indicate that LIG nano-delivery is a promising therapeutic approach for addressing DIC.

Conclusion The PHB2Ser91/Ser176 phosphorylation axis regulated by PIEZO1-TMBIM6 is an important target for LIG nano-drug delivery systems to improve mitochondrial damage in DIC.

Keywords Ligustrazine, Nano-carrier drug delivery, Doxorubicin-induced myocardial injury, Piezo-type mechanosensitive ion channel component 1, Prohibitin 2, Mitochondrial quality control

*Correspondence:
Yifeng Nie
nieyf@nanoctr.cn
Yingzhen Du
zhenzhen52@163.com
Hao Zhou
zhouhao@plagh.org
Xing Chang
xingchang_tcm@outlook.com
Full list of author information is available at the end of the article

© The Author(s) 2025. **Open Access** This article is licensed under a Creative Commons Attribution-NonCommercial-NoDerivatives 4.0 International License, which permits any non-commercial use, sharing, distribution and reproduction in any medium or format, as long as you give appropriate credit to the original author(s) and the source, provide a link to the Creative Commons licence, and indicate if you modified the licensed material. You do not have permission under this licence to share adapted material derived from this article or parts of it. The images or other third party material in this article are included in the article's Creative Commons licence, unless indicated otherwise in a credit line to the material. If material is not included in the article's Creative Commons licence and your intended use is not permitted by statutory regulation or exceeds the permitted use, you will need to obtain permission directly from the copyright holder. To view a copy of this licence, visit http://creativecommons.org/licenses/by-nc-nd/4.0/.

Graphical abstract

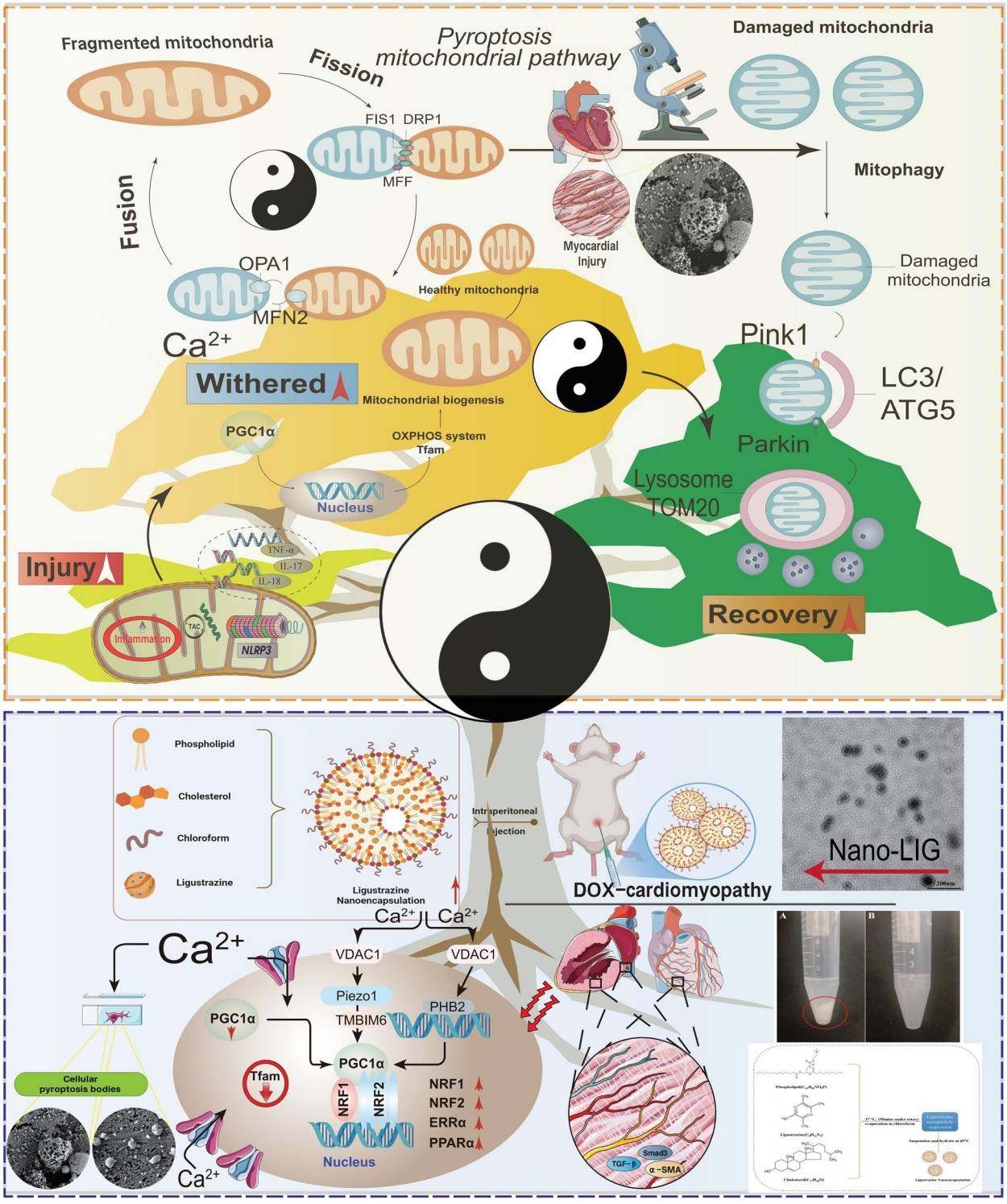

Background

Doxorubicin (DOX) is frequently exploited in clinical practice due to its broad-spectrum anticancer activity, high therapeutic efficacy, and robust antineoplastic properties [1, 2]. However, its clinical application is severely limited, as it induces myocardial injury, inflammatory storms, arrhythmias, and irreversible damage, that evolves into dilated cardiomyopathy and congestive heart failure [3, 4]. Acute or subacute cardiotoxic effects manifest during the early treatment phases, whereas chronic systolic dysfunction develops in a dose-dependent manner [5].

Mechanistic studies have identified mitochondrial oxidative stress, energy metabolism dysfunction, calcium dyshomeostasis, and toxic metabolite accumulation as the key contributors to DOX-induced cardiomyopathy (DIC) [6]. Moreover, programmed cell death mechanisms, including ferroptosis, pyroptosis, adenocarcinoma and necroptosis, further worsen DIC [7–10]. Mitochondria are the central regulators of cardiomyocyte homeostasis and the primary targets of DIC. The drug interacts with cardiolipin, a phospholipid enriched in the mitochondrial membranes, thereby facilitating mitochondrial accumulation [11, 12].

This relationship affects the respiratory chain complex activity, inhibits cardiac troponin and myosin light chain function, and lowers adenosine triphosphate (ATP) production. Concurrently, DOX-induced endoplasmic reticulum (ER) stress dysregulates sarcoplasmic reticulum Ca^{2+}-ATPase expression, thereby exacerbating calcium-handling defects and energy metabolism impairment [13, 14]. Chronic mitochondrial DNA damage and inhibition of respiratory complexes are associated with the development of delayed cardiomyopathy, whereas dysregulation of mitochondrial quality control has been linked to sepsis, endotoxemia, hyperglycemia, oxidative stress, and ischemia–reperfusion injury. Additionally, the involvement of the sirtuin 1-mediated mitochondrial unfolded protein response (UPR^{mt}) in DIC has been established, and cardioprotective drugs including apigenin, astragaloside IV, and quercetin have been investigated. Nonetheless, the therapeutic application of these natural chemicals is impeded by their inadequate bioavailability, fast disintegration, and limited aqueous solubility.

To address these limitations, a nanoparticle-based ligustrazine (LIG) delivery system was developed using tetrahedral framework nucleic acids (tFNA). The tFNA/LIG complex markedly improved drug solubility, prolonged systemic circulation, and enhanced stability with free LIG. The experimental results confirmed that nano-formulated LIG exhibited superior cardioprotective efficacy compared with that of conventional administration. Genetic and cellular models of DIC further elucidate the therapeutic mechanism of the LIG nano-drug delivery system. The modulation of the piezo type mechanosensitive ion channel component 1 (PIEZO1)/transmembrane BAX inhibitor motif containing 6 (TMBIM6)-prohibitin 2 (PHB2) phosphorylation axis restores mitochondrial quality control, inhibits cardiomyocyte pyroptosis, and alleviates myocardial dysfunction, thereby providing experimental evidence for the clinical potential of nanoparticle-delivered LIG as a targeted therapy for DIC.

PIEZO1 is a mechanosensitive ion receptor that transduces mechanical stressors into biochemical signals and is vital for several physiological functions [15]. As a critical mediator of mechanotransduction in humans, PIEZO1 is activated by mechanical stimuli that induce cell membrane deformation. Known agonists include Yoda1, Jedi1, and Jedi2 [15]. In the cardiovascular system, PIEZO1 regulates cardiac mechano-chemotransduction, shear stress sensing, and baroreceptor mechanosensitivity. Moreover, functional expression of PIEZO1 in cardiac fibroblasts exacerbates inflammatory injury and promotes pathological remodeling [16]. In addition to cardiac pathology, PIEZO1 activation in vascular endothelial and smooth muscle cells contributes to stress-induced vascular injuries. Systemic or endothelial-specific PIEZO1 knockout leads to lethal embryonic vascular malformations. Mechanistically, PIEZO1-mediated calcium influx drives hypertensive vascular remodeling and pressure overload-induced cardiac hypertrophy [17, 18]. Although PIEZO1 is recognized as a potential regulatory protein, the specific mechanisms underlying its involvement in DIC and downstream regulatory networks remain uncharacterized.

Mitochondrial quality surveillance (MQS), which encompasses mitophagy, dynamics, biogenesis, and unfolded protein response (UPR), maintains mitochondrial homeostasis and bioenergetic functions. This regulatory network coordinates inter-organelle communication to meet cellular energy demands. Cardiomyocytes, with their high mitochondrial density and limited mitochondrial motility, exhibit unique MQS characteristics [17]. MQS dysregulation was delineated in stress-induced cardiovascular injuries and therapeutic interventions targeting these pathways were validated. However, the interaction between PIEZO1-mediated ion channel activity and DOX-induced MQS impairment requires further systematic investigation. PHB2 governs mitophagy through its association with microtubule-associated protein 1 light chain 3 and modifies phosphatase and tensin homolog-induced kinase 1 (PINK1)/

parkin signaling via the presenilin-associated rhomboid-like protein-phosphoglycerate mutase family member 5 (PGAM5) pathway [19, 20]. In alcoholic cardiomyopathy, the PGAM5-PHB2 interaction induces PHB2Ser91 ($PHB2^{S91}$) phosphorylation, with phosphomimetic ($PHB2^{S91D}$) and phosphorylation-deficient ($PHB2^{S91A}$) mutants differentially affecting mitochondrial function. Transgenic $PHB2^{S91}$ phosphorylation confers cardiac dysfunction in murine models [21]. PHB2 also mitigates septic cardiomyopathy by maintaining dual specificity phosphatase 1 (DUSP1) activity to preserve phosphorylation-dependent mitophagy/ER-phagy coordination, thereby preventing pan-apoptotic activation and bioenergetic collapse [22, 23]. Pyruvate kinase M2 deficiency exacerbated inflammatory cardiomyocyte apoptosis, whereas PHB2 overexpression rescued mitochondrial biogenesis and functional integrity [24]. In acute kidney injury models, TMBIM6 governs mitochondrial PHB2 localization, and TMBIM6 overexpression reverses membrane potential loss and apoptosis. PHB2 knockout abolishes TMBIM6-mediated renal protection, thus confirming its functional interdependence [25].

Therefore, this study hypothesized that LIG nano-formulation ameliorates DIC through PIEZO1-mediated regulation of PHB2 phosphorylation at Ser91/Ser176 residues. This proposed mechanism involves TMBIM6-PHB2-dependent restoration of mitochondrial quality control networks, thereby effectively suppressing DIC pyroptosis. By delineating the targeted therapeutic effects and mitochondrial protective actions of the nano-formulation within the PIEZO1-PHB2 interaction framework, this study elucidated a novel pharmacological strategy to counteract chemotherapy-induced cardiotoxicity. These mechanistic insights provide a robust experimental foundation for developing precise therapies targeting mitochondrial homeostasis in DIC while highlighting the translational potential of nanoparticle-delivered LIG as a promising cardio-oncological agent.

Methods

Synthesis of LIG nanocapsule

Phospholipids, LIG, and cholesterol were uniformly combined in accordance with the experimental ratio and thereafter transferred to a 100-mL round-bottom flask. Subsequent to the incorporation of 30 mL of chloroform, the mixture underwent sonication. The solvent was subsequently eliminated using a rotary evaporator under vacuum at 37 °C, with a condensation reflux for 150 min to get the LIG nanoparticle suspension. Four milliliters of triple-distilled water was incorporated, and the suspension was hydrated at 65 °C for two hours. Subsequent to cooling in an ice bath, the combination underwent sonication for 5 min utilizing a cell disruptor (100 W with a pulse cycle of 2 s on and 3 s off). The combination was subsequently processed using a liposome extruder to yield the LIG nanocapsule, which was diluted as necessary for ensuing tests.

Characterization of LIG nanocapsule

A suitable volume of the produced sample was extracted and diluted, followed by the deposition of 10 μL of the diluted solution onto a 230-mesh carbon-coated copper grid for 15–20 min. The surplus liquid was absorbed with filter paper, after which a drop of 1% uranyl acetate solution was applied for negative staining in the dark for 10 min. The excess stain was thereafter eliminated, and the grid was rinsed three times with distilled water, each rinse lasting one minute. The grids were dried overnight, and the samples were examined using transmission electron microscopy (TEM). A nanoparticle analyzer was employed to assess the particle size distribution, dimensions, and zeta potential utilizing clean water as the solvent.

Stability assessment of LIG nanocapsule

The LIG nanocapsule prepared according to the optimized formulation was stored at room temperature. Samples were taken on days 0, 3, 7, and 10. The solutions' appearance, morphology, and solubility were examined, and the particle size distribution, dimensions, and zeta potential were quantified to assess alterations in these characteristics.

Raw data processing and analysis

Gene Expression Omnibus (GEO) datasets, specifically GSE76314 and GSE181517, were utilized for the analysis, and GSE181517 as the validation set [26]. Both datasets include six myocardial cell samples exposed to DOX and six normal myocardial cell samples. Data related to mitophagy-associated genes were retrieved from GenBank.

Single-cell RNA sequencing (scRNA-seq) sample preparation and data analysis

Heart tissue samples were obtained from three experimental groups: control, DIC, and DIC treated with Chuanxiong-based nanomedicine. The tissues were immediately placed in ice-cold PBS and subjected to enzymatic digestion using collagenase IV and elastase at 37 °C for 30 min to obtain single-cell suspensions. Following filtration through a 70 μm cell strainer, the suspension was further purified using density gradient centrifugation. Cell viability was determined by trypan

blue exclusion, with a threshold of > 85% for further analysis. The concentration was adjusted to approximately 1000 cells/μL for 10 × Genomics. Single-cell RNA sequencing libraries were prepared according to the 10 × Genomics Chromium Single Cell 3' v3 kit protocol. Briefly, single-cell suspensions were mixed with barcoded Gel Beads to form GEMs (Gel Bead-in-emulsions), followed by cell lysis, mRNA capture, reverse transcription, cDNA amplification, and library preparation. The quality of the libraries was assessed using an Agilent Bioanalyzer 2100, and sequencing was performed on an Illumina NovaSeq 6000 platform, achieving around 50,000 reads per cell. Raw sequencing data were processed using Cell Ranger (v6.1.2, 10 × Genomics) for quality control, alignment to the mouse reference genome (mm10), barcode identification, and UMI counting. Filtering was applied based on criteria of 200–6000 genes, 500–30,000 UMI counts, and < 15% mitochondrial gene content, resulting in approximately 8000–10,000 high-quality cells per sample. Data analysis was conducted using the Seurat package (v4.1.0) in the R environment (v4.1.2). Normalization was performed using the "LogNormalize" method, and the top 2000 highly variable genes were selected for principal component analysis. The first 30 principal components were chosen based on the elbow plot for dimensionality reduction and clustering. UMAP and Louvain clustering algorithms (resolution = 0.5) were applied for visualization and cell clustering. Cell types were identified using marker genes such as RyR2 for cardiomyocytes and Pecam1 for endothelial cells. Differential expression analysis was performed using Seurat's FindMarkers function with the Wilcoxon rank-sum test, with significance thresholds set at an adjusted p-value < 0.05 and |log2FC| > 0.5. Expression patterns of Piezo1 and Vdac1 were visualized using FeaturePlot and VlnPlot. Cells were classified based on Piezo1 expression levels, and gene ontology (GO) enrichment analysis and gene set enrichment analysis (GSEA) were conducted with the clusterProfiler package (v4.0.5). Heatmaps were generated using the pheatmap package, and gene expression correlations with pathway activity were visualized using ggplot2.

Nano LIG materials and reagents

LIG from Chengdu HerbSubstance Co., Ltd (Chengdu, China), along with various laboratory equipment such as a circulating water vacuum pump (Model: SHB-III, Zhengzhou Great Wall Scientific Industry and Trade Co., Ltd., Zhengzhou, China), rotary evaporator (Model: RE-52A, Shanghai Yarong Biochemical Instrument Factory, Shanghai, China), and others, were utilized. A magnetic stirrer with water bath, liposome extruder, and nanoparticle size analyzer were also used for characterization and analysis. The following chemicals were employed: phospholipids, cholesterol, and chloroform, sourced from respective suppliers in China.

Synthesis and characterization of LIG nanocapsule

Phospholipids, LIG, and cholesterol were weighed according to the experimental ratio and placed in a 100-mL round-bottom flask. Chloroform (30 mL) was added, and the mixture was sonicated for 10 min at 100 W. A rotary evaporator was then used to remove the solvent under vacuum at 37 °C for 150 min. Following this, 4 mL of triple-distilled water was added, and the suspension was hydrated at 65 °C for 2 h. After cooling in an ice bath, the mixture was sonicated for 5 min using a cell disruptor. The solution was then passed through a liposome extruder to obtain the LIG liposome solution. For characterization, 10 μL of the solution was placed onto a carbon-coated copper grid, stained with 1% uranyl acetate, and observed under a transmission electron microscope. The particle size distribution and zeta potential were analyzed using a nanoparticle analyzer with pure water as the solvent.

Molecular and protein docking

Molecular docking simulations were done to study the interactions between LIG and many putative protein targets. The selected protein targets were PIEZO1, TMBIM6, and PHB2. These proteins are closely associated with cellular stress responses, mitochondrial function, and autophagy regulation, and are likely involved in the biological effects of LIG. Protein docking is an important computational biology method used to predict the interactions between proteins. The three-dimensional structures of target proteins were first retrieved from the Protein Data Bank database and preprocessing was performed using MOE and PyMOL tools. This procedure comprised the removal of water molecules, insertion of hydrogen atoms, and minimization of energy to ensure protein stability. Simultaneously, the three-dimensional structures of the ligand molecules were optimized using tools such as ChemAxon Marvin Sketch. Docking was conducted using AutoDock Vina with appropriate docking boxes set to define the binding regions, and binding energies were calculated using the scoring functions. Finally, the results were visualized using PyMOL and Chimera, focusing on hydrogen bonds and hydrophobic interactions to assess binding affinity. By combining molecular dynamics simulations, the stability of the docking conformations was further validated, thus providing valuable theoretical support for drug design and functional research.

Animals

All experimental methods involving animals were conducted in strict conformity with the National Institutes of Health (NIH) Guide for the Care and Use of Laboratory Animals. The study protocols were evaluated and approved by the Institutional Animal Ethics Committee of the Guangzhou University of Chinese Medicine (approval no. GZTCMF-20230097). The mice were housed under regulated environmental circumstances with a 12-h light/dark cycle, and all animals received ad libitum access to conventional rodent feed and water. No extra grouping or treatment was applied to the genetically engineered mice during the trial period.

Cardiomyocyte-specific conditional *Piezo*1- and *Tmbim6*-knockout models ($PIEZO^{Cko}$ and $TMBIM6^{Cko}$) were generated by crossing *Piezo*1- and *Tmbim6*-flox/flox ($TMBIM6^{f/f}$ and $PIEZO1^{f/f}$) mice with α-myosin heavy chain (α-MHC)-Cre transgenic mice. Age-matched $PIEZO1^{f/f}$and $TMBIM6^{f/f}$ littermates were used as wild-type controls. As previously described [22], PHB2 phosphorylation site-specific mutants ($PHB2^{S91A/S91D/S176A/S176D}$) were created by Cyagen Biosciences (Santa Clara, CA, USA). The DIC model was created via the intraperitoneal injection of DOX (D1515, Sigma-Aldrich, St. Loius, MI, USA) at 12.5 mg/kg dissolved in saline and administered as a single dose, following known protocols [25]. The control group received an equivalent volume of saline. At week 7 post-injection, mice satisfying the predetermined cardiac dysfunction criteria were selected for experimental analysis. Therapeutic interventions comprised dose-escalation studies comparing traditional free LIG administration with nanoparticle-encapsulated formulations of 25 mg/kg/day (low), 50 mg/kg/day (mid), and 100 mg/kg/day (high) for 14 days.

For animal sampling, the animals were fasted for 4–6 h before the experiment to eliminate influence from gastrointestinal contents. Sodium pentobarbital (50 mg/kg, intraperitoneally) was given for anesthesia. Before the heart was removed, the mouse was placed supine on an anatomical plate (under constant temperature), and the limbs were fixed. The chest and abdomen were disinfected with 75% alcohol. Thereafter, the chest was cut open and scissors were used to cut the skin along the midline (from the jaw to pubic symphysis). Subsequently, both sides of the rib arch were cut laterally, the sternum was turned up, and a beating heart was observed. The apex of the heart was gently lifted using forceps, and the pulmonary vein, aorta, and superior and inferior vena cavae were cut. The heart was quickly removed and placed in pre-cooled phosphate-buffered saline (PBS) to wash off the blood stains. After perfusion and fixation with 4% paraformaldehyde and 2.5% glutaraldehyde, the samples were used for pathological analysis and transmission electron microscopy, and liquid nitrogen quick freezing at − 80 ℃ was applied for subsequent molecular biology experiments.

Cell experiments and interventions

The HL-1 murine cardiomyocyte cell line was sourced from the Experimental Animal Center of Guangzhou University of Chinese Medicine. Cells were grown in low-glucose Dulbecco's Modified Eagle's Medium (DMEM; Corning Cellgro, Corning, NY, USA), supplemented with 10% fetal bovine serum (Atlanta Biologicals, Atlanta, GA, USA) and 1% penicillin/streptomycin (Invitrogen, Carlsbad, CA, USA). To establish an in vitro model of DIC, HL-1 cells were pretreated with 1 μM DOX for 24 h. Primary cardiomyocytes were isolated from the neonatal hearts of $PIEZO1^{f/f}$, $TMBIM6^{f/f}$, $PIEZO1^{Cko}$, $TMBIM6^{Cko}$, $PIEZO1^{TG}$, and $TMBIM6^{TG}$ mice using standard enzymatic dissociation protocols. The isolated cells were then subjected to treatments such as small interfering RNA (siRNA)-mediated knockdown (si-PHB2/si-TMBIM6), adenoviral overexpression (ad-PHB2/ad-TMBIM6), or modulation of site-specific phosphorylation ($PHB2^{S91A/S91D/S176A/S176D}$), according to the experimental design.

For adenoviral transduction, cardiomyocytes were seeded into 24-well plates at a density of $5–10\times10^4$ cells per well. Transfection was initiated when cells reached 30–40% confluence, with viral vectors applied for 14 h before replacing the medium with fresh DMEM. Transfection efficiency was evaluated at 72 h post-transduction using PCR and Western blot analysis. Forty-eight hours before the experimental endpoint, primary cardiomyocytes were co-cultured with either 1 μM DOX or PBS as a vehicle control. The therapeutic strategies included dose-escalation trials comparing traditional free LIG administration with nanoparticle-encapsulated formulations and treatment regimens tailored to specific genetic and pharmacological subgroups. LIG concentrations were 25 μmol/L (low), 50 μmol/L (mid), and 100 μmol/L (high).

To specifically activate the PIEZO1 ion channel or inhibit mitophagy, cardiomyocytes in respective experimental groups were pretreated for 4 h with either the PIEZO1 channel agonist Yoda1 (5 μM) or the selective mitophagy inhibitor 3-methyladenine (10 mM) prior to subsequent analyses. These pharmacological treatments were employed to explore the roles of mechanosensitive signaling and mitochondrial quality control pathways in DOX-induced cardiotoxicity [25].

Small animal echocardiography

Cardiac functional assessment was performed using echocardiography to evaluate left ventricular ejection fraction (LVEF) alterations across the experimental

groups post-DOX injury and therapeutic intervention. Following induction of anesthesia with 3% isoflurane, the mice were maintained under 1.5% isoflurane during imaging. Animals were positioned supine on a thermostatically controlled platform (37 ℃) to preserve physiological body temperature. The thoracic region was carefully depilated, and high-resolution images were acquired using a 30-MHz transducer (VisualSonics Vevo 3100, Fujifilm, Minato, Japan) with an ultrasonic coupling gel. Parasternal long-axis views were captured during steady-state respiration to minimize motion artifacts, and LVEF was calculated using the Simpson's biplane method [22].

TEM evaluation

Myocardial mitochondrial morphology was analyzed according to established protocols [22]. Briefly, the cardiac tissues were fixed in 2.5% glutaraldehyde/2% paraformaldehyde, post-fixed with 1% osmium tetroxide, and embedded in epoxy resin. Ultrathin sections (70 nm) were stained with uranyl acetate/lead citrate and analyzed using a JEM-1400Plus TEM (JEOL, Minato, Japan) equipped with a VELETA CCD camera (Olympus, Shinjuku, Japan). Mitochondrial cristae density, matrix clarity, and outer membrane integrity were quantified across ≥ 50 fields per group using ImageJ v1.53.

Histopathological evaluation

Formalin-fixed myocardial tissues were paraffin-embedded, sectioned at 4-μm thickness, and stained with hematoxylin–eosin for general morphology or trichrome staining according to the Masson method for collagen deposition analysis. The fibrosis area (%) was calculated as collagen-positive regions relative to the total myocardial area using NIS-Elements BR software (Nikon Eclipse 80i, Nikon, Minato, Japan) across five randomized fields per slide [27].

Immunofluorescence staining

Fresh cardiac tissues were quickly frozen in optimal cutting temperature compound (− 80 °C). Cryosections (4 μm) were fixed with 4% paraformaldehyde, permeabilized using 0.5% Triton X-100, and blocked with 10% goat serum. Primary antibodies (listed in Supplementary Table 1) were incubated overnight at 4 °C, followed by incubation with Alexa Fluor-conjugated secondary antibodies (1:500, 1 h). Nuclei were stained with 4',6-diamidino-2-phenylindole. Fluorescence images were obtained using an LSM 510 confocal microscope (Carl Zeiss, Oberkochen, Germany) with standardized exposure settings [28].

Cell counting kit-8 (CCK8) and enzyme-linked immunosorbent assay (ELISA)

Cardiomyocyte viability in different experimental groups was assessed with the CCK8 assay according to the manufacturer's instructions. Oxidative stress markers (malondialdehyde, glutathione, and catalase) and antioxidant enzyme activities in cardiomyocytes or cardiac tissues were measured using ELISA kits (NeoBioscience Technology, Shenzhen, China). Additionally, the levels of the anti-inflammatory cytokine interleukin (IL)-10 and pro-inflammatory cytokines IL-17 and IL-18 were quantified using ELISA kits from the same supplier [23].

Western blot analysis

Protein extracts from cardiomyocytes and cardiac tissues were prepared following standard procedures. Cellular lysates were obtained using tissue protein extraction reagent (Thermo Fisher Scientific, Waltham, MA, USA) and centrifuged at 10,000×*g* for 20 min at 4 ℃. Cardiac tissue lysates were prepared by homogenizing 75 mg of frozen tissue in radioimmunoprecipitation assay buffer containing protease/phosphatase inhibitors, followed by centrifugation at 14,000×*g* for 30 min at 4 °C. Protein concentration was measured using the bicinchoninic acid assay, and equal amounts of protein (20 μg for cells, 50 μg for tissues) were separated by 10% sodium dodecyl sulfate–polyacrylamide gel electrophoresis. Proteins were transferred to polyvinylidene difluoride membranes (MilliporeSigma, Burlington, MA, USA) and incubated with primary antibodies (listed in Supplementary Table 1) overnight at 4 °C. Membranes were then incubated with horseradish peroxidase-conjugated secondary antibodies (1:1000 dilution) for 1 h at room temperature, and signals were visualized using enhanced chemiluminescence reagents (Pierce, Rockford, IL, USA). Band intensity was analyzed using ImageJ software (NIH) [22].

Quantitative real-time PCR

Total RNA from frozen cardiac tissues or cultured cardiomyocytes was extracted using TRIzol reagent. Complementary DNA was synthesized using reverse transcriptase according to the manufacturer's protocol. Real-time PCR was performed with SYBR Green Master Mix (Roche, Basel, Switzerland) on a QuantStudio 5 system (Applied Biosystems, Waltham, MA, USA), using the following cycling conditions: 95 °C for 10 min, followed by 40 cycles of 95 °C for 15 s and 60 °C for 1 min. Relative gene expression was calculated using the ΔΔCt method, with glyceraldehyde-3-phosphate dehydrogenase as the endogenous control. Primer sequences are provided in Supplementary Table 2 [28, 29].

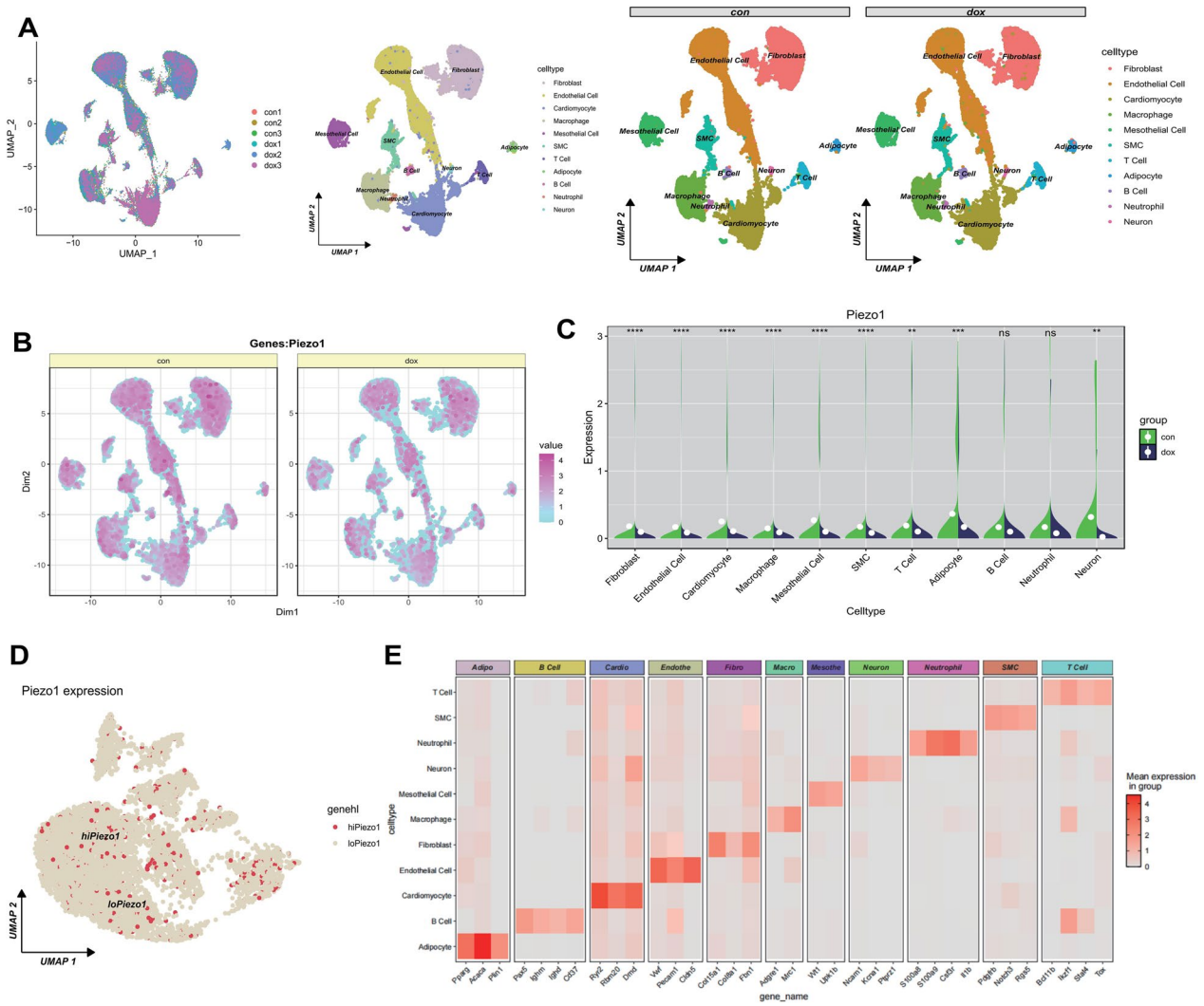

Fig. 1 Piezo1 as a critical therapeutic target in doxorubicin-induced cardiomyopathy. Single-cell transcriptomic profiling reveals Piezo1 dysregulation in DOX-induced cardiac injury. **A**–**C** UMAP projections of myocardial cell clusters from control (Con) and DOX-treated groups, annotated based on lineage-specific marker genes and feature plot visualization demonstrates spatial expression heterogeneity of Piezo1 across myocardial regions. **D** Stratification of cardiomyocyte subpopulations by Piezo1 expression median reveals differential activation patterns between Piezo1-high and Piezo1-low subgroups. **E** Heatmap validation of cluster-defining markers, confirming cellular identity assignments through canonical gene expression signatures (e.g., Tnnc1 for cardiomyocytes, Col1a1 for fibroblasts)

Statistical analysis

Data are expressed as mean ± standard deviation. Statistical analysis was performed using GraphPad Prism 9.0. Comparisons between two groups were made using the unpaired Student's t-test, while comparisons across multiple groups were analyzed using one-way analysis of variance with Bonferroni post hoc testing (for homogeneous variance) or Tamhane's T2 method (for heterogeneous variance). Statistical significance was set at $p < 0.05$. Additionally, comparisons between groups were made using an independent samples t-test, assuming normal distribution and homogeneous variance ($p > 0.05$, confirmed by Shapiro–Wilk and Levene tests). The significance level was set at $p < 0.05$, and mean differences and 95% confidence intervals were calculated.

Results

PIEZO1 is an important therapeutic target for DIC

To explore the mechanisms of DIC and to identify effective therapeutic targets, single-cell RNA sequencing (scRNA-seq) was used to analyze cellular population changes in DOX-treated and untreated cardiomyopathy mouse models. Heart tissues from different groups (Control, DIC, and DIC treated with a Chuanxiong-based

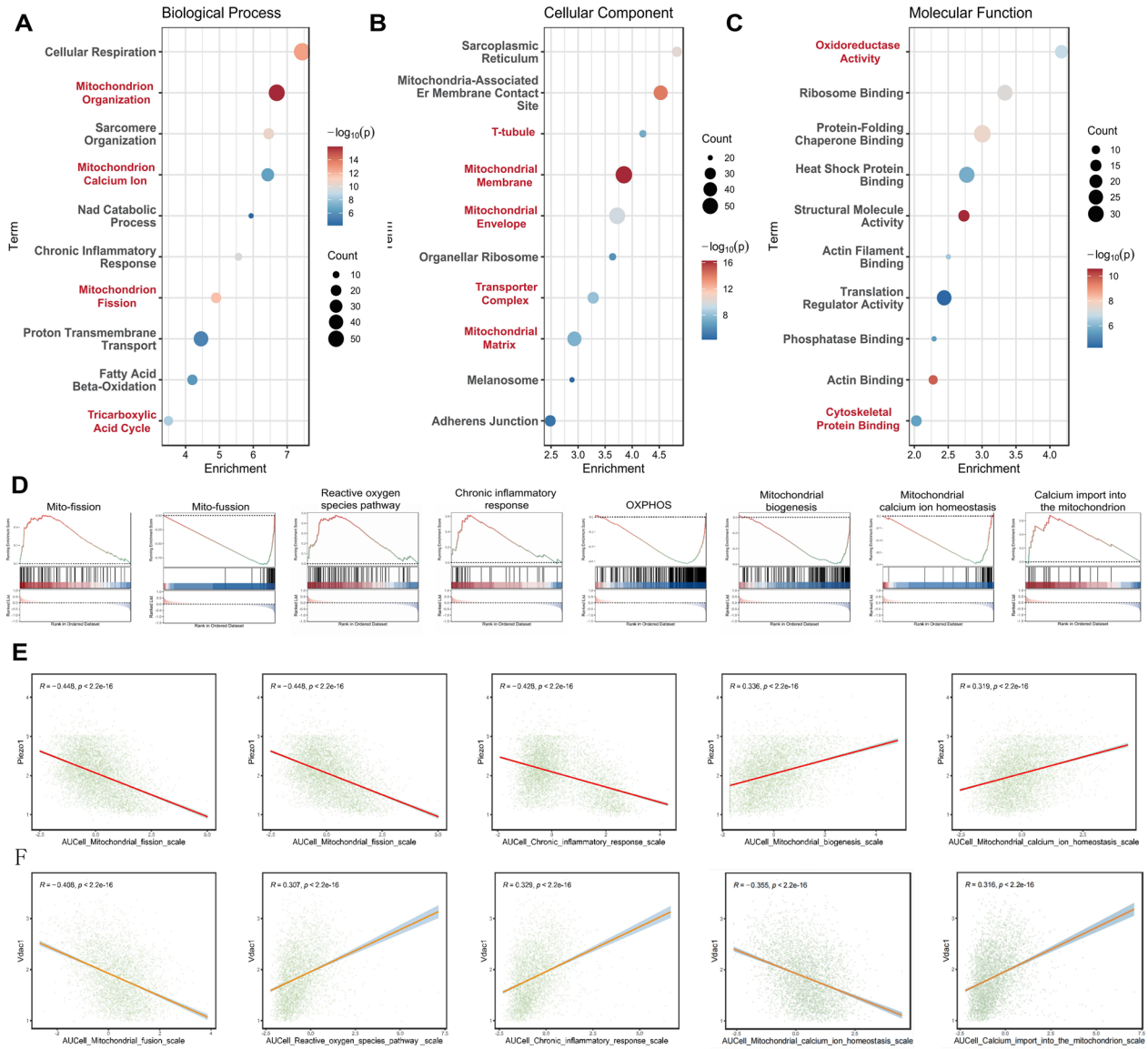

Fig. 2 Piezo1-mediated mitochondrial quality control dysregulation underlies doxorubicin cardiotoxicity. Integrated multi-omics analyses delineate the regulatory role of Piezo1 in mitochondrial homeostasis disruption. **A**–**C** Gene Ontology (GO) enrichment analyses of differentially expressed genes between Piezo1-high and Piezo1-low cardiomyocyte subpopulations demonstrate significant enrichment in mitochondrial membrane organization (biological processes), respiratory chain complexes (cellular components), and calcium ion binding (molecular functions). **D** Gene Set Enrichment Analysis (GSEA) further confirms the coordinated downregulation of oxidative phosphorylation and cristae formation pathways in Piezo1-high cells. **E**, **F** Correlation matrices reveal strong positive associations between Piezo1/Vdac1 expression levels and mitochondrial permeability transition pore activity scores, establishing a mechanistic link between calcium dyshomeostasis and quality control failure. These findings collectively implicate Piezo1 as a master regulator of mitochondrial integrity loss during chemotherapy-induced cardiac injury

nanomedicine intervention) were subjected to bioinformatics analysis.

A detailed analysis of single-cell transcriptomic data from a DIC model was conducted, with a focus on the differential expression of PIEZO1 and voltage-dependent anion-selective channel 1 (VDAC1) and their potential regulatory roles in myocardial cell metabolism. First, cellular subpopulations were defined based on the Uniform Manifold Approximation and Projection plot derived from the scRNA-seq data (Fig. 1A, B). By comparing the cell clusters between the control and DIC groups, multiple distinct cell populations, including cardiomyocytes, endothelial cells, and macrophages, were successfully identified. Each cluster was named and categorized based on specific marker genes, such as ryanodine receptor 2 for cardiomyocytes

and platelet and endothelial cell adhesion molecule 1 for endothelial cells, providing clear cell type information for subsequent analyses (Fig. 1G). Further analysis revealed the differential expression of PIEZO1 and VDAC1 across different cell subpopulations. Figure 1C shows the distribution of PIEZO1 expression in control and DIC groups. Feature plots demonstrate substantial dysregulation of PIEZO1 expression in the DOX group. Differential expression of PIEZO1 and VDAC1 across subpopulations was further validated using violin plots comparing the expression levels in various cell types between the control and DIC groups (Fig. 1D–G). These results suggested that PIEZO1 and VDAC1 play important roles in the pathophysiology of DIC.

To further investigate the molecular differences between cardiomyocytes with high and low PIEZO1 expression, gene ontology (GO) enrichment analysis was performed to explore the specific regulatory mechanisms of PIEZO1 in DIC (Fig. 2A–C). GO analysis revealed considerable differences between the high and low PIEZO1 expression groups in terms of various biological processes. These processes were enriched in "cellular respiration\mitochondrion organization and mitochondrial calcium ion homeostasis" as well as in "chronic inflammatory response and fatty acid beta-oxidation." At the cellular component level, differentially expressed genes were markedly enriched in mitochondria-related terms, such as "mitochondrial membrane, mito-ER membrane contact site, and mitochondrial envelope" (Fig. 2A–D), thus further suggesting that PIEZO1 may play a critical role in regulating mitochondrial function.

Additionally, gene set enrichment analysis (GSEA) supported the differential expression between the high and low PIEZO1 groups in metabolic pathways (Fig. 2D), particularly in those associated with mitochondrial dynamics, calcium homeostasis, oxidative stress, oxidative phosphorylation, and chronic inflammation. These findings aligned with earlier enrichment results, thereby reinforcing the notion that the PIEZO1 ion channel pathway is a critical target in mediating DIC.

Dysregulation of PIEZO1-mediated mitochondrial quality control is an important phenotype involved in DIC

The correlation between PIEZO1 and VDAC1 expression and the activity scores of related pathways were further analyzed (Fig. 2E–F). The results demonstrated a substantial correlation between PIEZO1 and VDAC1 expression and the activity scores of the enriched pathways in differential analysis, especially those related to mitochondrial function and cellular metabolism. These findings validate the potential roles of PIEZO1 and VDAC1 in the regulation of myocardial cell metabolism. In addition, these results provide important insights into the functional roles of PIEZO1 and VDAC1 in DIC and offer a new perspective for future research on the metabolic mechanisms underlying cardiomyopathies.

Moreover, GSEA further emphasized the involvement of mitochondrial dynamics (mitochondrial fusion/fission), biogenesis, calcium overload, and inflammatory injury mechanisms in DIC. DIC was strongly correlated with PIEZO1 and VDAC1 processes. This suggests that compared with that of control mice, DOX-treated mice showed enhanced regulation of PIEZO1- and VDAC1-mediated ion channels, which are closely associated with mitochondrial quality control phenotypes (Fig. 2A–E). To validate the pathological mechanisms and potential therapeutic targets, a database analysis was performed and mitochondrial transcription factors and inflammatory injury-related genes involved in DIC were identified. Using the GSE76314 dataset, 15 differentially expressed mitochondrial-related genes (deMRG) were identified. Using machine learning models, a generalized linear model (GLM) was validated using the validation dataset GSE181517. Enrichment analysis revealed strong associations between inflammatory responses and mitochondrial transcription factor A (TFAM) (Supplementary Materials 3A–3H).

Overall, single-cell sequencing and bioinformatic analysis revealed that PIEZO1-mediated mitochondrial quality control dysfunction is a crucial factor in DIC. Therefore, targeting the PIEZO1 ion channel pathway in cardiomyocytes shows the potential for therapeutic intervention in DIC. Furthermore, gene expression analysis revealed that PIEZO1-related pathways, such as mitochondrial structural damage, mitochondrial calcium homeostasis, mitochondrial fission, and the tricarboxylic acid cycle, may be essential therapeutic targets for DIC. These findings strongly suggest that PIEZO1-mediated mitochondrial quality control dysfunction is a key phenotype in the pathophysiology of DIC.

LIG nano-drug delivery system targets PIEZO1-mediated inflammatory injury and pyroptosis to treat DIC

A LIG nano-delivery system was constructed using four components (phospholipids, cholesterol, chloroform, and LIG). Phospholipids, LIG, and cholesterol were uniformly mixed according to the experimental ratios in a round-bottom flask using chloroform as the dispersant. The mixture was subjected to sequential processes, including ultrasonic mixing, rotary evaporation, condensation reflux, and hydration in an ice bath. Finally, the mixture was passed through a liposome extruder to obtain LIG nanocapsules, thereby establishing the

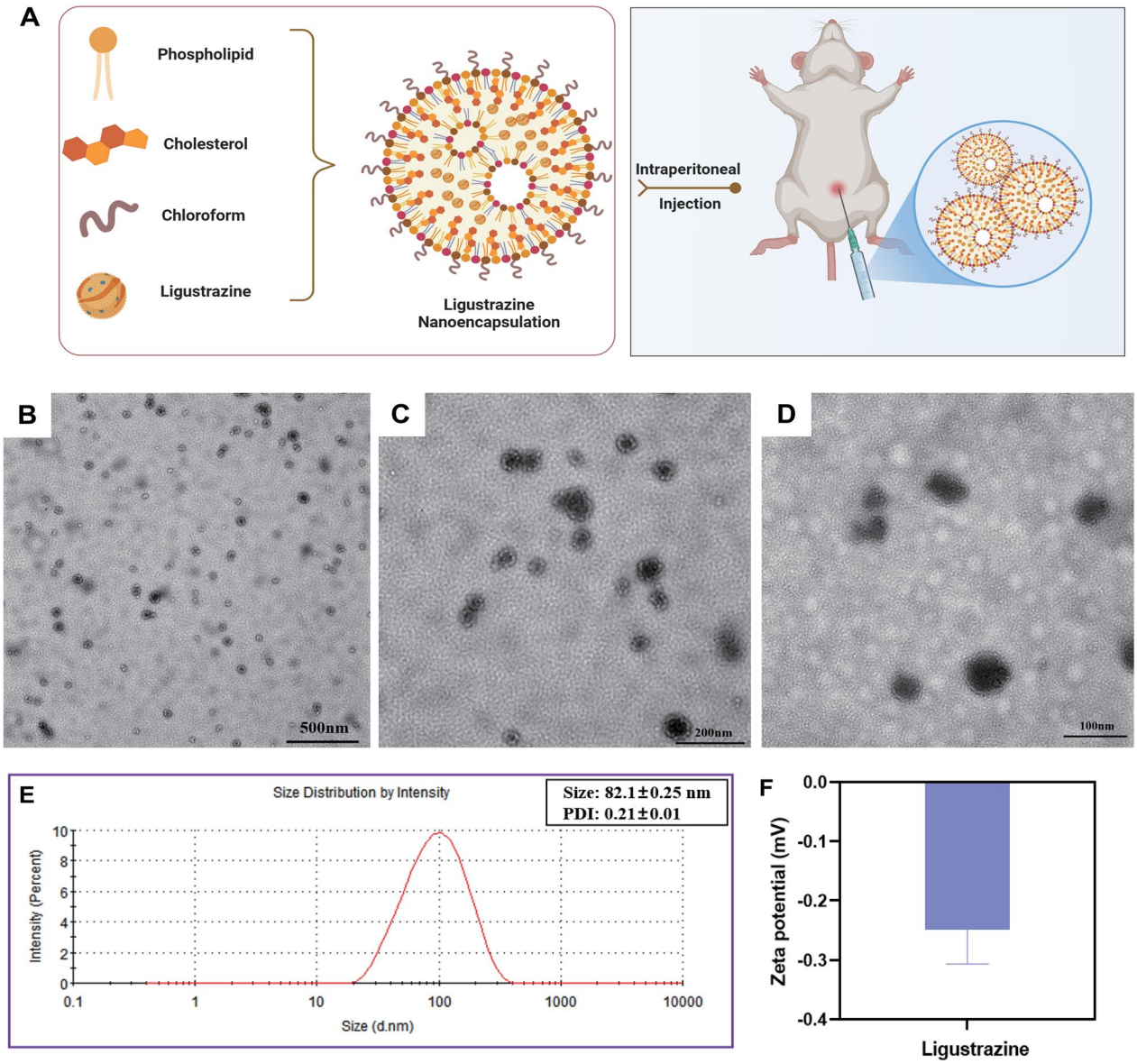

Fig. 3 The process and characterization of ligustrazine nanoencapsulation. **A** The schematic diagram of ligustrazine nanoencapsulation into nanoparticles involves the preparation process using a microencapsulation device to combine four components (phospholipids, cholesterol, chloroform and ligustrazine) into each formulation. After intraperitoneal injection for systemic administration, the nanoparticles are used to treat doxorubicin-mediated tumor cardiomyopathy. Representative transmission electron microscope images showing the morphology of Ligustrazine Nanoencapsulation. **B** Scale bar: 500 nm, **C** 200 nm, **D** 100 nm. The size distribution (**E**) and zeta potential (**F**) of Ligustrazine Nanoencapsulation. **A** Schematic representation of the tetramethylpyrazine (LIG)-loaded nanocarrier system, engineered through self-assembly of phospholipids, cholesterol, chloroform, and LIG for intraperitoneal administration in treating doxorubicin-induced cardiotoxicity. **B**-**D** Transmission electron microscopy (TEM) images validate the monodisperse spherical morphology of LIG nanoparticles at varying magnifications (Scale bars: 500 nm, 200 nm, and 100 nm, respectively). **E** Dynamic light scattering analysis demonstrates optimal hydrodynamic diameter (82.1 ± 0.25 nm) and narrow size distribution (polydispersity index [PDI] = 0.21 ± 0.01). **F** Zeta potential measurements confirm colloidal stability with a surface charge of − 0.249 ± 0.047 mV

LIG nano-delivery system for subsequent experiments (Fig. 3A–F, S1A–S1E).

To validate the therapeutic efficacy of this nano-delivery system, a DIC mouse model was established. In non-genetically modified mice, the DOX-treated group exhibited considerable myocardial pathological alterations, aggravated fibrosis, impaired cardiac ejection function, and enhanced neutrophil-mediated inflammatory injury (Fig. 4A–F). Concurrently, DIC demonstrated elevated transcription levels of pyroptosis-related

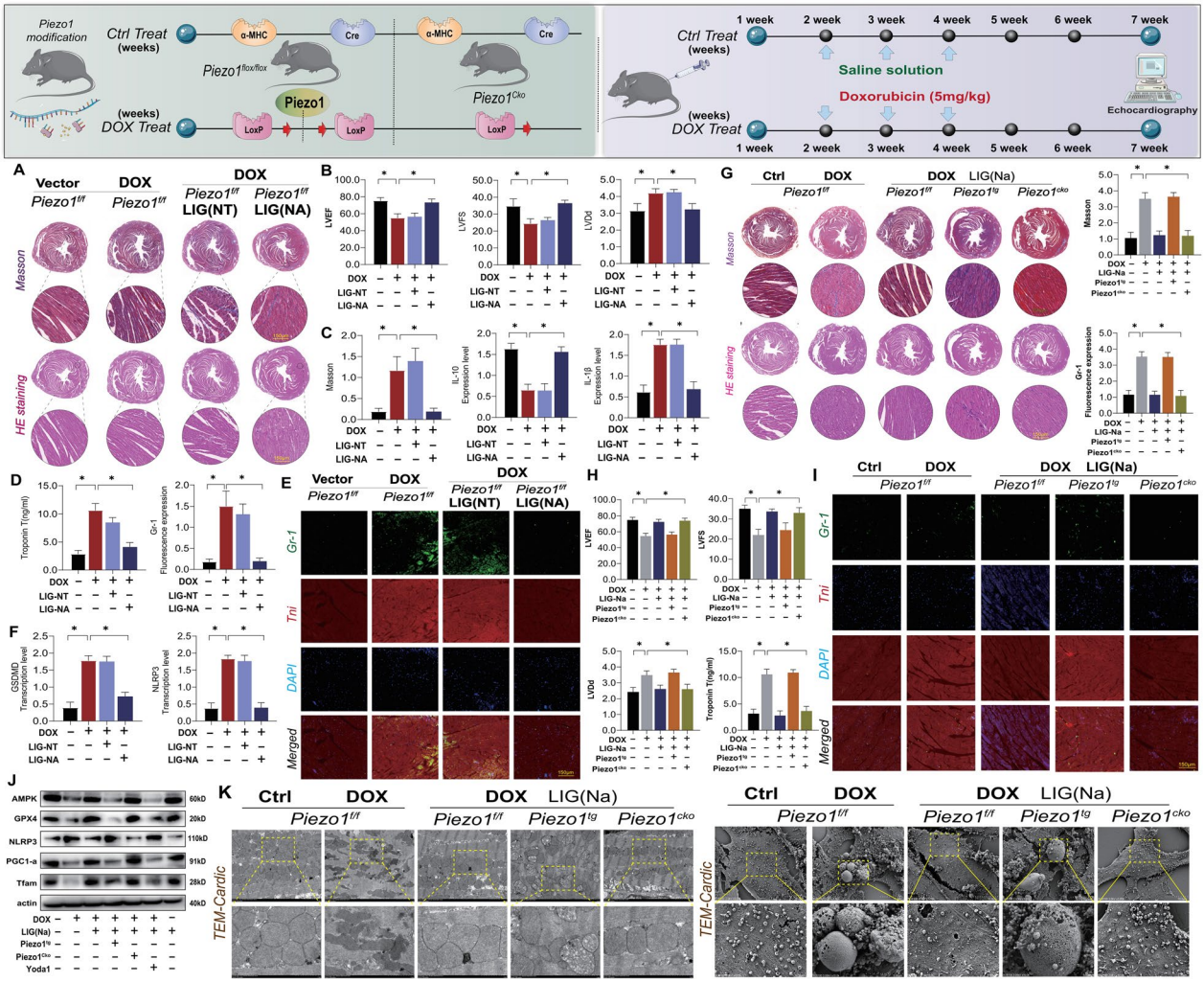

Fig. 4 The tetramethylpyrazine nano-drug delivery system treats doxorubicin-nduced myocardial injury by targeting piezo1-mediated inflammatory injury and pyroptosis. **A** Trichrome staining according to the Masson method and hematoxylin–eosin (H&E) staining reveal DOX-induced myocardial fibrosis and histopathological damage. **B** Echocardiographic analysis of cardiac function parameters: left ventricular ejection fraction (LVEF), left ventricular fractional shortening (LVFS), and left ventricular diastolic dimension (LVDd). **C** ELISA quantification of anti-inflammatory cytokine IL-10 and pyroptosis-related IL-1β transcript levels. **D**, **E** Immunohistochemical assessment of neutrophil infiltration (Gr-1 + cells) Troponin-T (Trop-T) expression levels as a biomarker of cardiomyocyte injury. **F** Transcript levels of pyroptosis-associated genes GSDMD and NLRP3. **G** Comparative histopathological analysis of myocardial fibrosis using trichrome staining according to the Masson method and hematoxylin–eosin (H&E) staining. **H** Echocardiographic re-evaluation of LVEF, LVFS, and LVDd with concomitant Trop-T quantification. **I** Secondary validation of Gr-1 + neutrophil infiltration in myocardial sections. **J** Western blot analysis of AMPK, GPX4, NLRP3, PGC1α, and TFAM protein expression. **K** Transmission electron microscopy (TEM) of myocardial ultrastructure and High-magnification TEM imaging of apoptotic bodies in cardiomyocytesValues are presented as mean ± SD. All experiments were conducted at least three times. *p < 0.05

genes (IL-1β, gasdermin D, nucleotide-binding domain, leucine-rich–containing family, pyrin domain–containing-3). Conventional administration of free LIG failed to reverse myocardial fibrosis, inflammatory injury, or pyroptosis. In contrast, the LIG nano-delivery system ameliorated fibrosis and inflammation, suppressed pyroptosis, and substantially improved cardiac ejection function in DOX-treated mice (Fig. 4A–F), thus indicating the superior therapeutic advantages of the nano-formulation.

To further investigate the therapeutic targets of the LIG nano-delivery system in DIC, cardiomyocyte-specific *Piezo1*-knockout ($PIEZO1^{Cko}$) and transgenic ($PIEZO1^{TG}$) murine models were generated using Cre-LoxP technology. $PIEZO1^{Cko}$ mice were obtained by crossing α-MHC-Cre transgenic mice with $PIEZO1^{f/f}$ mice. Multidimensional evaluations revealed that

DOX-treated mice exhibited mitochondrial structural disintegration, reduced biogenesis, and expanded pyroptotic bodies, along with characteristic fibrosis and inflammatory injury (Fig. 4G–K). Although the LIG nano-delivery system effectively attenuated fibrosis, restored mitochondrial integrity, enhanced biogenesis, and inhibited pyroptosis in both $PIEZO1^{f/f}$ and $PIEZO1^{Cko}$ mice, these therapeutic effects were not observed in $PIEZO1^{TG}$ mice (Fig. 4G–K).

These results suggested that PIEZO1 channel activation plays a pivotal role in mediating DIC. Furthermore, the LIG nano-delivery system likely exerted its cardioprotective effects by modulating PIEZO1-dependent mitochondrial homeostasis, thereby suppressing the activation of the pyroptotic pathway.

LIG nano-drug delivery system regulates mitochondrial dynamics (fusion/fission) through the PIEZO1 ion channel

The therapeutic advantages of the LIG nano-delivery system and its mechanism of regulating DOX-induced mitochondrial homeostasis and pyroptosis through PIEZO1 have been confirmed. To further validate the upstream targets and downstream phenotypes of this nano-formulation for DOX-mediated mitochondrial injury, genetic modifications of Piezo1 were carried out in primary cardiomyocytes isolated from genetically modified mice. DOX treatment induced marked reductions in cardiomyocyte viability and mitochondrial membrane potential, accompanied by suppressed mitochondrial biogenesis and disrupted cytoskeletal protein morphology (Fig. 5A and E). The LIG nano-delivery system reversed these pathological changes and restored the cell viability, mitochondrial membrane potential, and cytoskeletal integrity. However, conventional LIG administration has no regulatory effect on mitochondrial damage. Notably, PIEZO1 overexpression abolished the therapeutic efficacy of the nanoformulation in DIC, whereas PIEZO1-specific knockdown (sh-PIEZO1) did not affect its cardioprotective effects (Fig. 5A and E, Fig. S2A–2F).

To further explore the therapeutic potential of the Nano-delivery system, we assessed its effects on mitochondrial dynamics, encompassing fission/fusion processes and mitophagy. The findings demonstrated that DIC led to significant disruption of mitochondrial structure, manifested by increased fragmentation, reduced mitochondrial length, upregulated expression of fission-related proteins (such as dynamin-related protein 1 [DRP1], mitochondrial fission 1 [FIS1], and mitochondrial fission factor [Mff]), and decreased levels of fusion mediators (optic atrophy 1 [OPA1], mitofusin [MFN]1 and 2) (Fig. 5B–D). The LIG nanoformulation restored the mitochondrial dynamic balance by suppressing pathological fission, enhancing fusion activity, and preserving ultrastructural integrity. PIEZO1 overexpression nullified these regulatory effects, whereas PIEZO1 knockdown (sh-PIEZO1) did not impair therapeutic outcomes. Conventional LIG administration failed to mitigate the mitochondrial dynamic imbalance or pathological fission exacerbation (Fig. 5B–D).

LIG nano-drug delivery system regulates PINK/parkin-mediated mitophagy and UPR through PIEZO1 ion channel

Under various stress conditions, mitochondrial dynamics imbalance or excessive pathological fission often leads to mitophagy dysfunction in cardiomyocytes [30–32]. Accumulated dysfunctional mitochondrial fragments impair autophagosome-lysosome fusion, thereby suppressing mitochondrial self-renewal capacity, inhibiting biogenesis, and reducing nascent mtDNA synthesis [33]. In DIC, mitophagy was significantly impaired, as indicated by a decrease in translocase of outer mitochondrial membrane 20 (TOM20) fluorescence intensity, downregulation of PINK1/parkin transcription, and reduced mitophagy indices. The LIG nano-formulation [LIG (Na)] intervention reversed these abnormalities by restoring PINK1/parkin-mediated mitophagy, enhancing TOM20 expression, and normalizing mitophagy activity (Fig. 5F–G and Fig. S4A–S4B). Notably, *Piezo1* overexpression abolished the regulatory effects of LIG (Na) on mitophagy, whereas *Piezo1* knockdown (sh-Piezo1) did not attenuate its efficacy. Conventional LIG administration [LIG (NT)] failed to rescue mitophagy defects (Fig. 5F, G and Fig. S4A–S4B).

The study findings further demonstrated that stress-induced mitochondrial hyperfission and mitophagy insufficiency were accompanied by exacerbated UPR^{mt}, oxidative stress, and inflammatory activation. DOX injury markedly suppressed the respiratory chain complex activity (complexes I/III/IV/V) (Fig. S4C–S4D). LIG (Na) treatment attenuated UPR^{mt} overactivation and oxidative damage while restoring respiratory complex expression and energy metabolism. LIG (Na) exhibited superior therapeutic efficacy to LIG (NT) in modulating these pathological pathways (Fig. S4C–S4D). Collectively, these results indicate that LIG (Na) alleviates DIC by PIEZO1-dependent restoration of mitochondrial dynamic balance and mitophagy-UPR^{mt} synergy, ultimately rescuing respiratory chain functionality and bioenergetic metabolism [34].

The LIG nano-drug delivery system targets $PHB2^{S91/S176}$ sites via the PIEZO1 ion channel

The preliminary findings confirmed that aberrant PIEZO1 expression contributes to DOX-mediated dysregulation of mitochondrial quality control networks

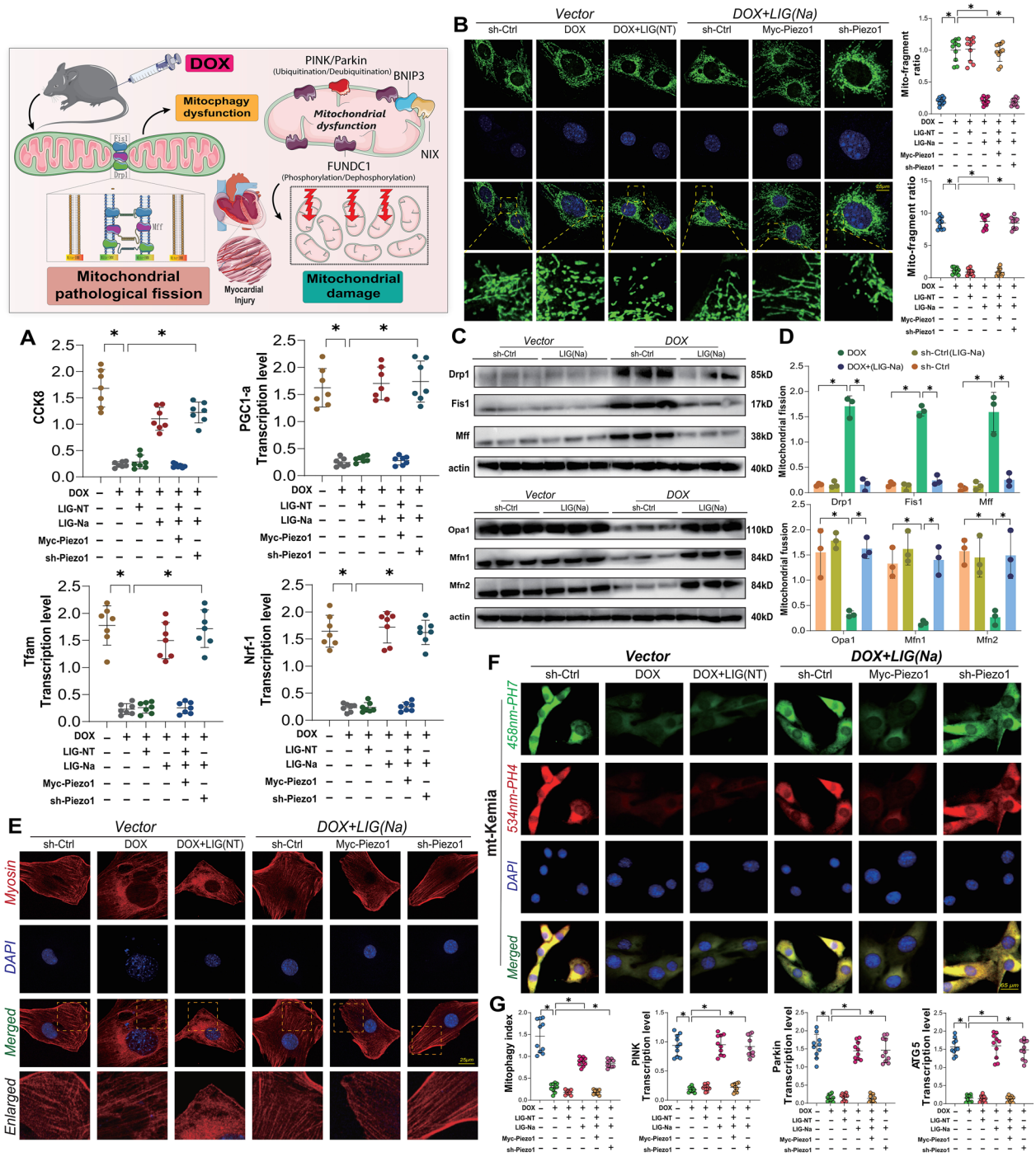

Fig. 5 The tetramethylpyrazine nano-drug delivery system regulates mitochondrial quality control via the Piezo1 ion channel and alleviates doxorubicin-induced cardiomyocyte injury. **A** Cell viability assessed by Cell Counting Kit-8 (CCK8) assay and Transcript levels of mitochondrial biogenesis regulators (PGC1α, TFAM, NRF1); **B** Mitochondrial network integrity visualized via MitoTracker staining; **C**, **D** Expression of mitochondrial fission drivers (DRP1, MFF, FIS1) and Expression of mitochondrial fusion mediators (OPA1, MFN1, MFN2); **E** Confocal laser scanning microscopy of cardiomyocyte cytoskeletal architecture (α-actinin/vinculin co-staining); **F**, **G** Quantitative analysis of mitophagy flux and PINK1, PARKIN, and ATG5 transcript levels

in cardiomyocytes. To further identify the downstream regulatory proteins of PIEZO1 in mitochondrial dysfunction, cardiomyocyte models were established with the following site-specific PHB2 phosphorylation modifications: phosphomimetic mutants ($PHB2^{S91D}$/$PHB2^{S176D}$) and phosphorylation-deficient mutants ($PHB2^{S91A}$/$PHB2^{S176A}$), followed by LIG (Na) intervention. The combined $PHB2^{S91A}$ (dephosphorylation mimic) and $PHB2^{S176D}$ (phosphorylation mimic) modifications pronouncedly exacerbated DOX-induced mitochondrial membrane potential loss, suppressed respiratory chain and energy metabolism functions, and disrupted mitochondrial dynamics (Fig.S5A–S5E). Non-modified cardiomyocytes exhibited similar pathological changes (Fig. S5A–S5E), indicating that $PHB2^{S91/S176}$ phosphorylation status is a critical therapeutic target for LIG (Na) in mitigating DOX-induced mitochondrial injury.

To determine whether PIEZO1 regulates $PHB2^{S91/S176}$ phosphorylation, PIEZO1 transgenic mice (Myc-PIEZO1) were generated and DOX intervention followed by PHB2 phosphorylation-specific modifications in isolated primary cardiomyocytes was performed. DOX pretreatment induced severe mitochondrial dysfunction, characterized by reduced activity, exacerbated pathological fission, suppressed respiratory complex levels, impaired mitophagy, and abnormal UPRmt activation (Fig. 6A–E, Fig. S8A–8 K). LIG (Na) treatment substantially attenuated mitochondrial fission, restored mitophagy and respiratory complex activity, and suppressed UPR^{mt} overactivation. However, sh-PHB2 and $PHB2^{S176}$ phosphorylation mimicry abolished these therapeutic effects, whereas $PHB2^{S91}$ modifications did not impair the mitochondrial protection conferred by LIG (Na) (Fig. 6A–E, Fig. S8A–8K). Notably, both $PHB2^{S91}$ and $PHB2^{S176}$ phosphorylation modifications in Myc-PIEZO1 cardiomyocytes disrupted the efficacy of LIG (Na). This suggests that PIEZO1 was essential for regulating PHB2 phosphorylation and mediating the mitochondrial protective effects of the nano-formulation.

Further experiments revealed that LIG (Na) reversed DOX-induced abnormal activation of the UPRmt and preserved cytoskeletal integrity (Fig. 6F, G). Consistent with previous findings, $PHB2^{S176}$ phosphorylation mimicry blocked these therapeutic effects, whereas $PHB2^{S91}$ modifications had no effect. PIEZO1 activation via Yoda1 treatment similarly disrupted the efficacy of LIG (Na) in both $PHB2^{S91}$- and $PHB2^{S176}$-modified models (Fig. 6F, G), thus confirming that PIEZO1 is an upstream regulator of PHB2 phosphorylation at these sites.

LIG nano-drug delivery system regulates $PHB2^{S91/S176}$ phosphorylation via PIEZO1-TMBIM6 pathway to modulate mitochondrial-ER homeostasis

To validate the regulatory role of PIEZO1 in $PHB2^{S91/S176}$ phosphorylation, cardiomyocyte-specific *Piezo1*-knockout mice ($PIEZO1^{Cko}$) were generated and primary cardiomyocytes were isolated for PHB2 phosphorylation-specific modifications. Post-DOX injury analysis revealed considerable upregulation of VDAC1 and mitochondrial fission drivers (DRP1, FIS1, and MFF), along with downregulation of fusion mediators (OPA1 and MFN2) (Fig. 6A, B). LIG (Na) treatment effectively suppressed fission protein expression and restored fusion mediator levels. However, $PHB2^{S176}$ phosphorylation mimicry abolished these therapeutic effects, whereas $PHB2^{S91}$ modifications showed no interference (Fig. 6A, B). Notably, neither sh-PIEZO1 nor the combined $PHB2^{S91/S176}$ phosphorylation modifications impaired the efficacy of LIG (Na) (Fig. 6A, B). This confirmed that PIEZO1 is an upstream regulator of PHB2 phosphorylation and a critical therapeutic target.

The role of TMBIM6 in the modulation of PHB2 phosphorylation and mitochondria-associated pathology has been established. To elucidate the pathways downstream of LIG (Na) via PIEZO1, *Tmbim6*-transgenic (Myc-TMBIM6) and -knockout (sh-TMBIM6) mouse models were developed. Analysis of the GSE76314 [35] (training set) and GSE181517 [36] (validation set) GEO datasets identified 15 deMRGs. Machine learning model validation (GLM) revealed strong associations with the mitochondrial fusion mediator OPA1, respiratory chain subunit nicotinamide adenine dinucleotide dehydrogenase iron-sulfur (NDUFS4), and biogenesis factor TFAM (Fig. S3A–S3H). Experimental validation confirmed that LIG (Na) could reverse the suppression of NDUFS4, TFAM, and peroxisome proliferator-activated receptor gamma coactivator 1α transcription induced by DOX, as well as restore the balance of mitochondrial dynamics (OPA1/DRP1/FIS1). Overexpression of Myc-TMBIM6 and Myc-PIEZO1 abolished these effects, whereas genetic knockouts did not impair the therapeutic action of LIG (Na) (Fig. S5K–S5P).

In TMBIM6 transgenic cardiomyocytes subjected to $PHB2^{S91/S176}$ phosphorylation, DOX injury induced a marked reduction in cell viability, ER structural disintegration, and UPRmt overactivation (Fig. 6C–6E). LIG (Na) intervention restored ER integrity and suppressed the UPRmt; however, PHB2 phosphorylation mimicry attenuated these effects. Neither TMBIM6 overexpression nor *Piezo1* knockout influenced PHB2 phosphorylation status or counteracted the therapeutic outcomes of LIG (Na) (Fig. 6C–E). Collectively, these findings demonstrate that LIG (Na) mitigates DIC via

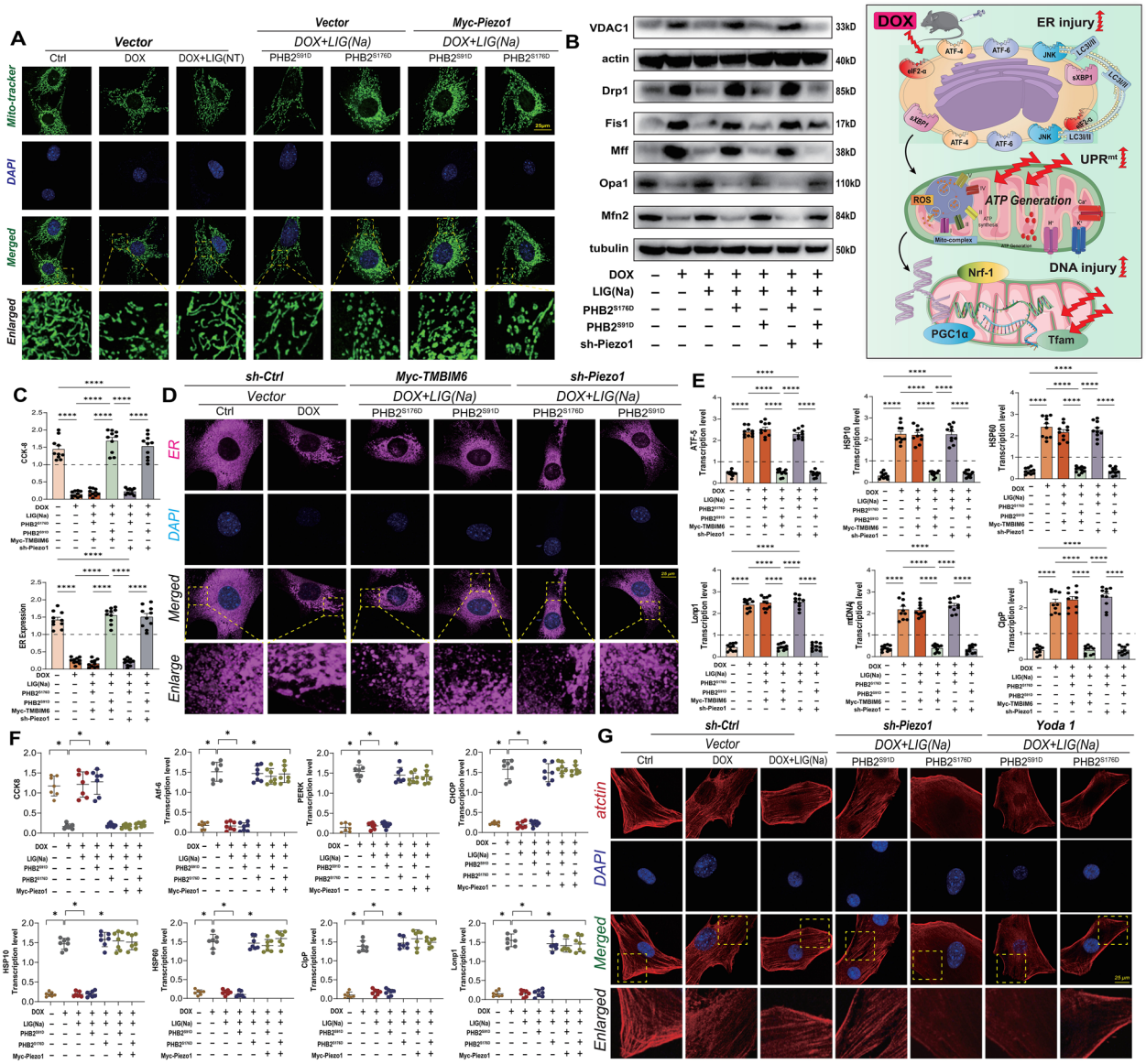

Fig. 6 Piezo1-mediated phosphorylation of PHB2 at ser91/Ser176 sites is an important pathway for the tetramethylpyrazine nano-drug delivery system in treating doxorubicin-induced cardiomyocyte injury. **A** Mitochondrial network integrity assessed by confocal laser scanning microscopy (MitoTracker Green FM; Scale bar: 20 μm); **B** Western blot quantification of VDAC1 protein expression and mitochondrial dynamics regulators (DRP1, MFF, FIS1, OPA1, MFN2); **C**, **D** Cardiomyocyte viability (CCK8 assay) and ER ultrastructure visualization (ER-Tracker Red); **E** Secondary validation of UPRmt markers (ATF5, HSP10, HSP60, mtDNAj, LONP1, CLPP); **F** Cardiomyocyte viability (CCK8 assay) and qPCR analysis of UPRmt effectors (ATF6, PERK,HSP10, HSP60, CHOP, LONP1, CLPP); **G** Immunofluorescence imaging of cytoskeletal proteins (α-actinin/desmin); Values are presented as mean ± SD. All experiments were conducted in triplicate. *p < 0.05

(See figure on next page.)

Fig. 7 The tetramethylpyrazine nano—drug delivery system regulates the phosphorylation at PHB2$^{S91/S176}$ sites via the Piezo1—TMBIM6 pathway to modulate the coordinated mitochondrial—endoplasmic reticulum autophagy, thereby inhibiting pyroptosis. **A** ER structural integrity evaluated via confocal microscopy (ER-Tracker™ Red staining; Scale bar: 10 μm). **B**–**E** Cell viability (CCK8 assay) combined with respiratory chain complex activity (Complex I/II) and transcript quantification of mitochondrial stress markers (CLPP, HSP10, HSP60, PERK, LONP1) and mitophagy regulators (PINK1, PARKIN, ATG5). **F** Western blot analysis of mitophagy effector proteins (ATG5, PINK1, PARKIN, TOM20) and mitochondrial inner membrane translocase (TIM23). **G** Quantitative analysis of mitophagy flux; Values are presented as mean ± SD. All experiments were conducted in triplicate. *p < 0.05

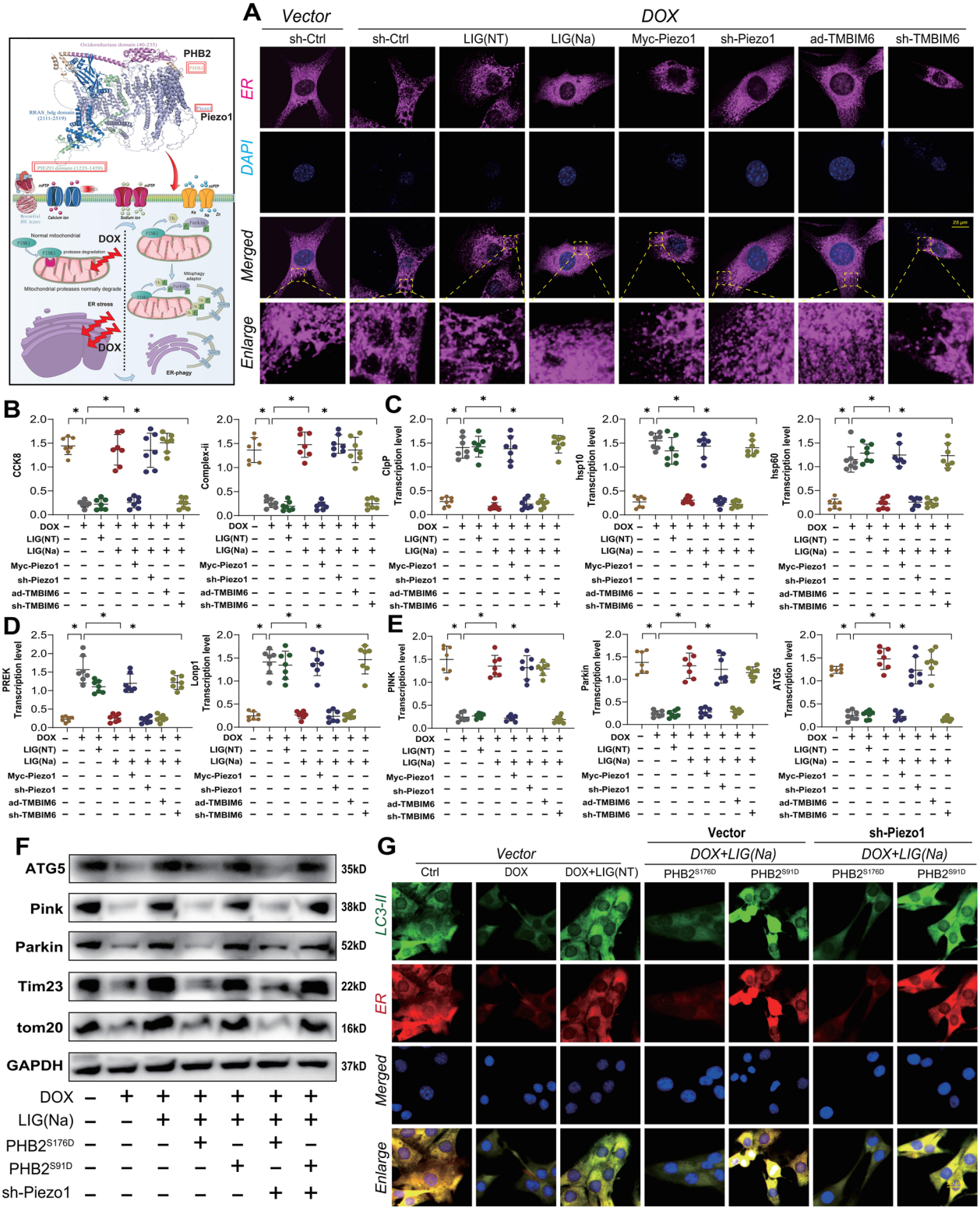

Fig. 7 (See legend on previous page.)

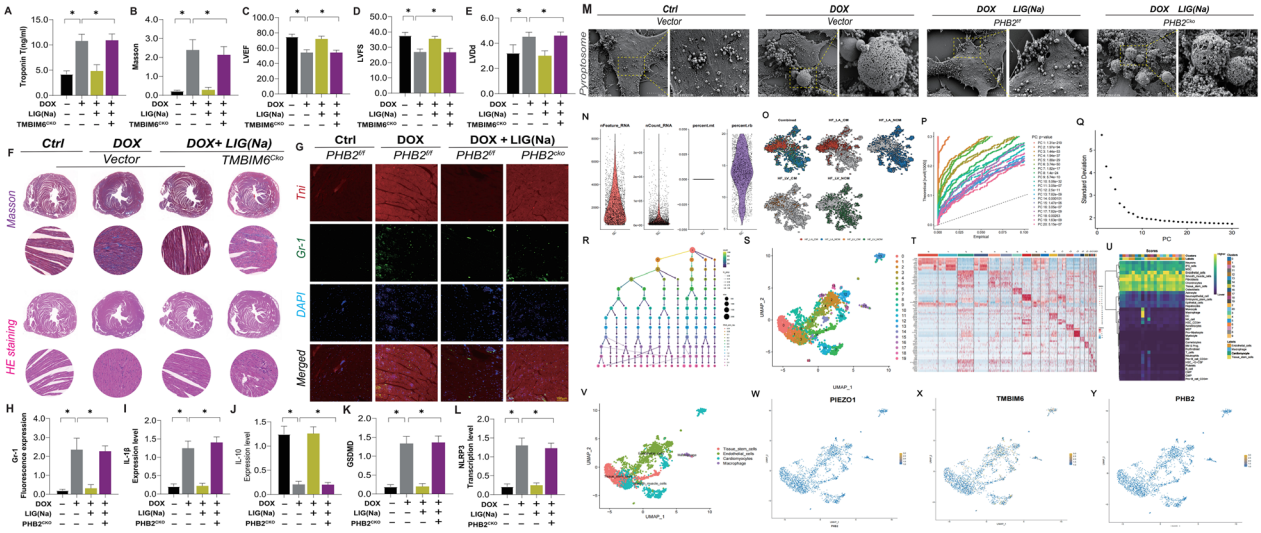

Fig. 8 The tetramethylpyrazine nano-drug delivery system improves myocardial inflammatory injury and pyroptosis through the TMBIM6-PHB2 pathway. **A** Myocardial expression levels of Troponin T (ng/mL). **B**–**F** Representative histopathological and Masson images (H&E and Masson staining) showing myocardial disarray in Adriamycin induced myocardial injury mice. **F** Echocardiographic analysis of cardiac functional parameters, including left ventricular ejection fraction (LVEF), left ventricular fractional shortening (LVFS), and left ventricular diastolic. **G**, **H** Tissue fluorescence detection of myocardial neutrophil inflammatory injury; **I**–**L** Detection of anti-inflammatory factor IL-10 expression levels and pyroptosis-related gene transcription levels; **M** Detection of pyroptotic bodies in myocardial tissue. **N**–**Y** Analysis of single-cell database for the correlation between PIEZO1-TMBIM6-PHB2 and doxorubicin-inducediomyopathy; Values are presented as mean ± SD. All experiments were conducted in triplicate. *$p < 0.05$

the PIEZO1-TMBIM6 axis, thereby regulating PHB2$^{S91/S176}$ phosphorylation to restoring mitochondrial-ER functional coordination.

LIG nano-drug delivery system regulates PHB2 $^{S91/S176}$ phosphorylation via PIEZO1-TMBIM6 pathway to modulate mitochondrial-ER autophagy

Using single-cell sequencing public databases, PIEZO1-TMBIM-PHB2 was identified as an important regulatory pathway of DOX-induced myocardial injury that mediated cardiomyocyte injury through the mitochondrial pathway (Fig. 8N–Y). To investigate the role of the PIEZO1-TMBIM6-PHB2 axis and the therapeutic mechanisms of LIG (Na) in DIC, genetic modifications, including overexpression of Myc-PIEZO1/Myc-TMBIM6 and knockdown of sh-Piezo1/sh-TMBIM6, were conducted in DIC. Confocal microscopy and molecular analyses revealed that DOX injury induced structural disintegration of the ER, exacerbated UPR^{mt} activation, and suppressed mitophagy/ER-phagy coordination (Fig. 7A–G, Fig. S7A–S7J). LIG (Na) treatment restored these parameters, and this effect was abolished by sh-TMBIM6 or Myc-PIEZO1 overexpression (Fig. 7A–G, Fig. S7A–S7J).

PHB2$^{S91/S176}$ phosphorylation modulation experiments demonstrated site-specific regulatory effects; PHB2^{S176} phosphomimetic mutants (PHB2^{S176D}) blocked ERphagy restoration by LIG (Na), whereas PHB2^{S91} modifications showed no interference (Fig. 7A–G). PIEZO1 knockout did not affect the ability of LIG (Na) to modulate PHB2 phosphorylation or ER-phagy confirmed pathway independence from baseline PIEZO1 activity. In TMBIM6 cardiac-specific knockout (TMBIM6^{Cko}) mice, LIG (Na) failed to mitigate DOX-induced UPR^{mt} overactivation or pyroptosis (Fig. S7C–7J). Parallel in vitro studies established that Myc-PIEZO1/sh-TMBIM6 co-modulation nullified the therapeutic effects of LIG (Na) on mitophagy-UPR^{MT} coordination and mitochondrial dynamics (Fig. 7A–G). Similarly, dual genetic interventions (Myc-PIEZO1/sh-TMBIM6 and Myc-PIEZO1/ad-TMBIM6) abolished mitochondrial quality control restoration, thereby establishing PIEZO1-TMBIM6 as a master regulatory node (Fig. S6A–S6I).

Cardiac-specific TMBIM6 or PHB2 knockout mice exhibited complete resistance to the therapeutic effects of LIG (Na) on fibrosis, ejection fraction, and pyroptosis (Fig. 8A–M), thereby mirroring the PIEZO1^{Cko} phenotypes. These findings demonstrate that LIG (Na) alleviates DIC through PIEZO1-TMBIM6-mediated PHB2$^{S91/S176}$ phosphorylation, thereby restoring mitochondrial-ER functional synergy to suppress pathological remodeling.

Discussion

This study adopted a comprehensive approach combining nano-drug delivery, genetic modification, and single-cell sequencing to systematically investigate mitochondrial quality control dysfunction and the activation of cardiomyocyte pyroptosis in DOX-induced myocardial injury. The research sheds light on the complex interactions between PIEZO1-PHB2-mediated mitochondrial dysfunction and programmed cell death during DIC.

The LIG nano-formulation demonstrated superior cardioprotective efficacy compared with that of free LIG. The nano-formulation targeted the PIEZO1-TMBIM6 axis to activate PHB2 phosphorylation, thereby enhancing mitochondrial preservation. Single-cell sequencing revealed that the PIEZO1-gated channel-mediated disruption of mitochondrial-ER homeostasis is a critical therapeutic target for DIC. The nano-formulation restored mitochondrial dynamics through PIEZO1-PHB2-mediated regulation of PINK1/parkin-driven mitophagy, improved mitochondrial biogenesis, and alleviated excessive UPR caused by ER stress.

Mechanistically, pyroptosis activation occurs downstream of PIEZO1-PHB2-mediated mitochondrial quality control impairment, where DOX-induced oxidative inflammatory cascades and mitochondrial dysfunction collectively trigger the NLRP3 inflammasome pathway. This pathological process was effectively suppressed by LIG nano-treatment via modulation of TMBIM6-PHB2, and structural characterization confirmed direct PIEZO1-TMBIM6-PHB2 interactions that govern PHB2 phosphorylation at the Ser91/Ser176 residues. The nano-formulation precisely modulated this phosphorylation cascade to optimize mitochondrial quality surveillance.

Functional validation demonstrated PIEZO1-dependent mitochondrial translocation of TMBIM6, restoration of $PHB2^{S91}$ phosphorylation status, and subsequent enhancement of mitophagy-ERphagy coordination, ultimately promoting mitochondrial DNA stability and ATP synthesis while inhibiting DOX-induced pyroptosis. Therapeutic administration of the nano-formulation ameliorated myocardial pathological remodeling through PIEZO1-TMBIM6-PHB2-mediated mitigation of inflammatory/oxidative damage and restoration of cardiac contractile function. The PIEZO family constitutes the largest known mechanosensitive ion channels [15], with PIEZO1 functioning as a 300-kDa homotrimeric protein containing 2521 amino acids per glycosylated subunit. These evolutionarily conserved channels detect diverse mechanical stimuli including shear stress and matrix stiffness [17, 37]. PIEZO1, located on human chromosome 16, is a non-selective cation channel predominantly expressed in non-neuronal cells, with a strong preference for Ca^{2+} permeability [38]. Pathological activation under cytotoxic stimuli (ischemia, inflammation, or shear stress) induces calcium overload through pore-forming domains, subsequently triggering mechanotransduction pathways that disrupt organelle homeostasis (ER-mitochondrial crosstalk and UPR regulation) [22, 39, 40].

Emerging evidence highlights the multifaceted role of PIEZO1 in the pathogenesis of cardiac injury. Overexpression of PIEZO1 was observed in fibrotic liver tissues from both humans and mice with a macrophage-specific PIEZO1 knockout [45]. This exacerbated hepatic inflammation and fibrosis through impaired efferocytosis, which was confirmed using biomechanically mimetic culture systems [41]. PIEZO1 activation enhances phagosomal acidification and apoptotic debris clearance, thereby suppressing proinflammatory cytokine expression (e.g., TNF-α, IL-6) and promoting macrophage polarization toward anti-inflammatory phenotypes. Notably, systemic administration of the PIEZO1 agonist Yoda1 accelerated fibrosis resolution, highlighting its potential for therapy. Pharmacological studies further confirmed the cardioprotective effects of PIEZO1 targeting; quercetin mitigated ox-LDL-induced calcium overload in endothelial cells by modulating the PIEZO1-NF-κB/NLRP3 signaling pathway. Yoda1-induced PIEZO1 activation counteracted these protective effects, thereby confirming its target specificity. Based on these findings, this study established PIEZO1 as a central regulator of DIC, where it orchestrates mitochondrial ER damage networks through PHB2 phosphorylation cascades rather than directly disrupting ion channel homeostasis. This provides a novel therapeutic paradigm for targeting PIEZO1-PHB2 interactions.

Mitochondria are double-membrane organelles that govern oxidative phosphorylation and apoptotic regulation [42–44] and critically depend on PHB2 for structural and functional integrity [45–47]. The study data revealed that PHB2 deficiency exacerbated DIC by impairing the mitochondrial complex I-nicotinamide adenine dinucleotide dehydrogenase ubiquinone flavoprotein 2 interactions and membrane potential maintenance. This study further demonstrates that $PHB2^{S91/S176}$ phosphorylation dynamically regulates mitochondrial ER autophagy coordination, metabolic homeostasis through ATP synthesis, and pyroptosis susceptibility via NLRP3 inflammasome modulation. The LIG nano-formulation specifically restored the PHB2 phosphorylation status, effectively rebalancing mitochondrial fission/fusion dynamics, enhancing PINK1/parkin-mediated quality control, and suppressing the pathological UPR. Moreover, protein interaction analyses identified PIEZO1-TMBIM6 as an upstream regulator of PHB2 phosphorylation, with the nano-formulation modulating this network to preserve cardiac contractility and mitigate DOX-induced structural remodeling. These findings

collectively establish a multilevel regulatory mechanism through which the nanoengineered system achieves superior therapeutic efficacy in maintaining mitochondrial ER homeostasis and counteracting chemotherapy-induced cardiac dysfunction.

Extensive protein interaction studies have established PHB2 as a nodal regulator of diverse cardiac stress conditions. In alcoholic cardiomyopathy models, pathological upregulation of PGAM5 induces $PHB2^{S91}$ dephosphorylation, thereby exacerbating mitochondrial fission and impairing UPR regulation [33]. Cardiac-specific PGAM5 knockout reverses these abnormalities and enhances mitophagy and biogenesis [22]. Intriguingly, $PHB2^{S91}$ phosphomimetic mutations rescued mitochondrial dysfunction independent of PGAM5 inhibition, thus suggesting a phosphorylation-dependent regulatory autonomy. Parallel investigations in acute kidney injury models have revealed TMBIM6-mediated control of PHB2 mitochondrial localization. PHB2 ablation nullified the protective effects of TMBIM6 on membrane potential and permeability transition pore regulation, whereas the physical interaction between TMBIM6 and PHB2 via C-terminal/PHB domain binding facilitated mitochondrial translocation under stress conditions [29]. Ginsenoside Rb1 was identified as a TMBIM6-targeted cardioprotectant during ischemic injury. This natural compound modulates the DUSP1-TMBIM6 axis to suppress VDAC1 oligomerization, restore mitochondrial quality control, and mitigate inflammatory cascades [27, 29]. Consistently, TMBIM6 downregulation exacerbated LPS-induced septic cardiomyopathy, manifesting as exacerbated mitochondrial fragmentation, calcium dysregulation, bioenergetic failure, and pathologies reversed by transgenic TMBIM6 overexpression [48].

This study conducted an in-depth investigation based on these previous studies. Although the effectiveness of TMBIM6-VDAC1-PHB2 related targets has been preliminarily confirmed, the upstream mechanism has not been elucidated. Through gene modification experiments (in vitro and in vivo), this study established PIEZO1 as an upstream target of TMBIM6-VDAC1 that regulates downstream protein-mediated mitochondrial quality control and mitochondrial homeostasis. Moreover, downstream effectors of PIEZO1 were identified. Integrated pharmacology also revealed that the nano-drug loading system of LIG could further regulate TMBIM6-mediated mitochondrial quality control through PIEZO1, further inhibiting pyroptosis and myocardial injury via the mitochondrial pathway. In terms of experimental methods, PIEZO1, the main target of DOX myocardial injury, was screened using single-cell sequencing and further studied it as the main protein involved in LIG nano-targeted delivery. Furthermore, histological microscopic changes were observed in pyroptosomes before and after DOX myocardial injury using ultra-high-definition microscopy, which confirmed the mechanism of LIG nano-targeted delivery to inhibit cardiomyocyte pyroptosis.

This study extends these findings to DIC by demonstrating that TMBIM6 inactivation disrupts PHB2 phosphorylation at Ser91/Ser176, thereby impairing mitochondrial-ER crosstalk. Crucially, the LIG nano-formulation restored the TMBIM6-PHB2 interaction through PIEZO1-mediated signaling, achieving three therapeutic outcomes: preservation of organelle ultrastructural integrity, coordination of mitophagy-ERphagy synchronization, and inhibition of pathological cytoskeletal remodeling.

In vivo validation confirmed the dual regulatory capacity of the nano-formulation of independently modulating the TMBIM6 and PHB2 pathways while maintaining phosphorylation-dependent therapeutic specificity. $PHB2^{Ser91/Ser176}$ phosphomimetic mutations directly alter the target engagement efficacy of the nanoformulation, underscoring the centrality of these post-translational modifications in treatment response.

Mitochondria are the central hubs for cellular metabolic coordination and critically depend on dynamic membrane remodeling and quality control mechanisms to maintain functional integrity [49, 50]. Dysregulated mitochondrial dynamics, marked by excessive fission and inhibited fusion, drive the pathological accumulation of mitochondria, reduce mitophagy efficiency, and compromise mitochondrial DNA replication. These abnormalities exacerbate oxidative stress and bioenergetic failure through maladaptive UPR activation [51, 52]. Pharmacological interventions targeting mitochondrial quality control networks have demonstrated therapeutic potential by restoring fission/fusion equilibrium, synchronizing mitophagy-UPR coordination, and mitigating oxidative-metabolic dysfunction [53]. Notably, the TMBIM6-PHB2 axis has emerged as a conserved regulatory module across multiple organ injury models, orchestrating mitochondrial quality surveillance to suppress programmed cell death, including pyroptosis, ferroptosis, and necroptosis [48, 49]. In this study genetic engineering approaches systematically validated this regulatory axis and identified PIEZO1 as an upstream modulator, thereby elucidating the dual-targeting mechanism of the LIG nano-formulation for mitochondrial network restoration.

The ER is the primary intracellular calcium reservoir and undergoes stress-induced calcium dysregulation that propagates mitochondrial dysfunction through PIEZO1/VDAC1-mediated ion flux [54, 55]. Mitochondrial calcium overload activates matrix proteases, promotes the

overproduction of reactive oxygen species, and triggers the opening of mitochondrial permeability transition pores. These events collectively disrupt membrane potential and homeostasis of quality control [56]. The study data revealed that DIC simultaneously compromises ER-mitochondrial structural coupling and cytoskeletal architecture. The LIG nano-formulation counteracted these effects through coordinated organelle stabilization, thus effectively decoupling calcium-mediated crosstalk from apoptotic signaling.

Nanomedicines and targeted drug delivery systems, emerging as innovative models for drug administration, have demonstrated transformative effects in the precision treatment of various diseases, including cancer, cardiovascular disorders, and autoimmune conditions, due to their unique size-dependent properties and customizable functionalities. Natural product-derived small molecules continue to drive therapeutic innovation, with artemisinin, quercetin, astragaloside IV, and LIG demonstrating particular promise in preclinical cardiovascular research [23, 29, 54, 57]. Their multifaceted mechanisms, spanning ion channel modulation, redox balance restoration, and organelle protection, provide critical pharmacophores for the development of next-generation cardio-oncology agents.

LIG is a characteristic alkaloid derived from *Ligusticum chuanxiong* that exhibits multifaceted pharmacological properties. These properties include endothelial protection, antiplatelet aggregation, and antifibrotic effects, with established clinical applications in cardiovascular and cerebrovascular diseases [58–61]. However, the therapeutic potential of LIG is limited by its poor aqueous solubility, rapid systemic clearance, and limited myocardial targeting. To address these limitations, a nanoengineered drug delivery system was developed to substantially enhance the pharmacokinetic profile of LIG. By encapsulating LIG within biocompatible nanoparticles, this system achieves three critical improvements: an increased surface-area-to-volume ratio, which enhances the dissolution kinetics. The preclinical validation demonstrated the superior efficacy of the nano-formulation to free LIG in DIC models. Through integrated single-cell sequencing and genetic screening, PIEZO1-TMBIM6-PHB2 was identified as the core regulatory axis, with the nano-formulation specifically modulating mitochondrial ER quality control networks to suppress pyroptosis. Mechanistic studies confirmed its ability to restore PHB2 phosphorylation dynamics while maintaining cytoskeletal integrity, thereby outperforming conventional administration routes in terms of both therapeutic precision and duration.

Although this study has made considerable progress based on previous research, it has some limitations. First, the clinical drug metabolism and toxicity characteristics of the LIG nano-drug loading system was not validated through clinical experiments. In the future, the effectiveness and safety of this nano-drug loading system will be confirmed through multicenter and multi-sample clinical research. Due to constraints in experimental technology and resources, this study was unable to identify the interaction mechanism of PIEZO1-TMBIM6-PHB2 through co-immunoprecipitation and structural biology experiments. Future research will focus on further validating the interaction mechanism of PIEZO1-TMBIM6 and the phosphorylation pathways of $PHB2^{S91/S176}$ through complementary techniques, such as co-immunoprecipitation and structural biology, to comprehensively elucidate the PIEZO1-TMBIM6-PHB2 axis interaction. Finally, although single-cell sequencing analysis has positioned mitochondrial ER dysfunction as the core of DIC, the immunomodulatory effect of nano-formulations on myocardial macrophage-cardiomyocyte crosstalk remains unexplored. Therefore, future studies using spatial transcriptomics and organoid co-culture systems will delineate cell type-specific therapeutic responses, potentially revealing new secondary targets for combination therapies.

Conclusions

DIC triggered PIEZO1 pathway activation, which subsequently suppressed TMBIM6 expression and dysregulated $PHB2^{S91/S176}$ phosphorylation. Mechanistically, activated PIEZO1 directly interacts with TMBIM6 and PHB2 to induce pathological phosphorylation cascades, thereby disrupting mitochondrial-ER crosstalk and potentiating NLRP3 inflammasome-mediated pyroptosis. The LIG nano-formulation counteracted these effects by inhibiting PIEZO1 activation, thereby restoring physiological phosphorylation patterns at $PHB2^{S91/S176}$, and reestablishing mitochondrial quality control coordination with ER homeostasis. The study highlights a new therapeutic approach in cardio-oncology, where targeting the PIEZO1-TMBIM6-PHB2 axis involved in mitochondrial surveillance through nanoengineered drug delivery systems provides two key benefits: targeted molecular intervention and enhanced pharmacokinetic properties. This study provides critical experimental evidence for the development of mechanistically informed therapies for chemotherapy-induced cardiac complications, thereby bridging the gap between mitochondrial biology and clinical translation in oncological cardiovascular care.

Abbreviations

DOX	Doxorubicin
DIC	DOX-induced cardiomyopathy
LIG	Ligustrazine
PIEZO1	Piezo type mechanosensitive ion channel component 1
TMBIM6	Transmembrane BAX inhibitor motif containing 6

PHB2	Prohibitin 2
ATP	Adenosine triphosphate
ER	Endoplasmic reticulum
MQS	Mitochondrial quality surveillance
UPR	Unfolded protein response

Supplementary Information

The online version contains supplementary material available at https://doi.org/10.1186/s12951-025-03420-z.

Supplementary material 1.

Acknowledgements
This work was supported by grants from the National Natural Science Foundation of China (No. 82230126), the Project of Guangzhou Science and Technology Plan (2025A04J3964), Guang dong Provincial Key Laboratory of TCM Pathogenesis and Prescriptions of Heart and Spleen Diseases (2022B1212010012), the State Key Laboratory of Traditional Chinese Medicine Syndrome Projects (No.SKLKY2024B0001Z) and Beijing Natural Science Foundation JQ24046.

Author contributions
JY Wang, HW Zhuang, C Li and RQ Cai performed the experiments. Boxian Pang, Yukun Li, Sang-Bing Ong, Zhijiang Guo, Hongshuo Shi, Sicheng Zheng, Xinyong He, Zhongzheng Zhang, Xinxin Liu collected and analyzed all the data. Yifeng Nie and Yingzhen Du wrote and revised the original manuscript. Hao Zhou, Xing Chang organized all the images and provided regulatory and financial support throughout the entire project implementation. All the authors approved the submission of this manuscript.

Data availability
The data that support the findings of this study are available from the corresponding author upon reasonable request.

Declarations

Competing interests
The authors declare no competing interests.

Author details
[1]State Key Laboratory of Traditional Chinese Medicine Syndrome, School of Pharmaceutical Sciences, Guangzhou University of Chinese Medicine, Guangzhou 510006, Guangdong, China. [2]Liaoning University of Traditional Chinese Medicine, Shenyang 110032, Liaoning, China. [3]Shuguang Hospital Affiliated to Shanghai University of Traditional Chinese Medicine, Shanghai, China. [4]CAS Center for Excellence in Nanoscience, National Center for Nanoscience and Technology, Beijing 100190, People's Republic of China. [5]Department of Medicine & Therapeutics, Faculty of Medicine, The Chinese University of Hong Kong (CUHK), Hong Kong, SAR, China. [6]The Second Medical Center & National Clinical Research Center for Geriatric Diseases, Chinese PLA General Hospital, Medical School of Chinese PLA, Beijing 100853, China. [7]Senior Department of Cardiology, The Sixth Medical Center of People's Liberation Army General Hospital, Beijing 100048, China. [8]Guang'anmen Hospital, China Academy of Chinese Medical Sciences, Beijing 100053, China.

Received: 21 March 2025 Accepted: 27 April 2025
Published online: 27 May 2025

References

1. Teraoka K, Hirano M, Yamaguchi K, Yamashina A. Progressive cardiac dysfunction in adriamycin-induced cardiomyopathy rats. Eur J Heart Fail. 2000;2(4):373–8.
2. Pourmadadi M, Gerami SE, Ajalli N, Yazdian F, Rahdar A, Fathi-karkan S, Aboudzadeh MA. Novel pH-responsive hybrid hydrogels for controlled delivery of curcumin: overcoming conventional constraints and enhancing cytotoxicity in MCF-7 cells. Hybrid Adv. 2024;6: 100210.
3. Wu X, Wang Z, Liang Z, Li N, Chen J, Liu Q, Lei W, Wu X, Lu C, Deng C, Chen Y, Wang X, Wei J, Yang Y. Pleiotropic role of CCR9/CCL25 signaling in adriamycin-induced cardiomyopathy. J Adv Res. 2024;S2090–1232(24):00473–9.
4. Liao W, Rao Z, Wu L, Chen Y, Li C. Cariporide attenuates doxorubicin-induced cardiotoxicity in rats by inhibiting oxidative stress, inflammation and apoptosis partly through regulation of Akt/GSK-3β and Sirt1 signaling pathway. Front Pharmacol. 2022;13: 850053.
5. Xiao M, Tang Y, Wang J, Lu G, Niu J, Wang J, Li J, Liu Q, Wang Z, Huang Z, Guo Y, Gao T, Zhang X, Yue S, Gu J. A new FGF1 variant protects against adriamycin-induced cardiotoxicity via modulating p53 activity. Redox Biol. 2022;49: 102219.
6. Zong W-N, Yang X-H, Chen X-M, Huang H-J, Zheng H-J, Qin X-Y, Yong Y-H, Cao K, Huang J, Lu X-Z. Regulation of angiotensin-(1–7) and angiotensin II type 1 receptor by telmisartan and losartan in adriamycin-induced rat heart failure. Acta Pharmacol Sin. 2011;32(11):1345–50.
7. Wang J, Zhuang H, Yang X, Guo Z, Zhou K, Liu N, An Y, Chen Y, Zhang Z, Wang M, Chen J, Li C, Chang X. Exploring the mechanism of ferroptosis induction by Sappanone A in cancer: insights into the mitochondrial dysfunction mediated by NRF2/xCT/GPX4 axis. Int J Biol Sci. 2024;20(13):5145–61.
8. Sun R-L, Wang H-H, Gui Z-C, Shuang-Guo, Lin L-B, Fan J-X, Xue-Zhang, Mao B-Y, Liu G, Liu W-Z, Yue R-Z, Yin Y-L, Wang Q-Q, Li P. Protective effect of vitamin B6 against doxorubicin-induced cardiotoxicity by modulating NHE1 expression. J Biochem Mol Toxicol. 2023;37(10): e23403.
9. Zhou X, Wang H, Yan B, Nie X, Chen Q, Yang X, Lei M, Guo X, Ouyang C, Ren Z. Ferroptosis in cardiovascular diseases and ferroptosis-related intervention approaches. Cardiovasc Drugs Ther. 2024. https://doi.org/10.1007/s10557-024-07642-5.
10. Javad Javid-Naderi M, Valizadeh N, Banimohamad-Shotorbani B, Shahgolzari M, Shayegh F, Maleki-baladi R, Sargazi S, Fathi-karkan S. Exploring the biomedical potential of iron vanadate nanoparticles: a comprehensive review. Inorg Chem Commun. 2023;157: 111423.
11. Li Y, Yu J, Li R, Zhou H, Chang X. New insights into the role of mitochondrial metabolic dysregulation and immune infiltration in septic cardiomyopathy by integrated bioinformatics analysis and experimental validation. Cell Mol Biol Lett. 2024;29(1):21.
12. Pang B, Dong G, Pang T, Sun X, Liu X, Nie Y, Chang X. Advances in pathogenesis and treatment of vascular endothelial injury-related diseases mediated by mitochondrial abnormality. Front Pharmacol. 2024;15:1422686.
13. Zha W, Zhao Q, Xiao Y, Gan Y, Wei J, Yu M, Xu Y, Xu Q, Wu S, Yu W. Mitochonic acid 5 rescues cardiomyocytes from doxorubicin-induced toxicity via repressing the TNF-α/NF-κB/NLRP3-mediated pyroptosis. Int Immunopharmacol. 2023;123: 110736.
14. Zhou C, Yang Y, Hu L, Meng X, Guo X, Lei M, Ren Z, Chen Q, Ouyang C, Yang X. Effects of miR-143 regulation on cardiomyocytes apoptosis in doxorubicin cardiotoxicity based on integrated bioinformatics analysis. Toxicol In Vitro. 2023;93: 105662.
15. Zhao Q, Zhou H, Chi S, Wang Y, Wang J, Geng J, Wu K, Liu W, Zhang T, Dong M-Q, Wang J, Li X, Xiao B. Structure and mechanogating mechanism of the Piezo1 channel. Nature. 2018;554(7693):487–92.
16. Zhu W, Guo S, Homilius M, Nsubuga C, Wright SH, Quan D, Kc A, Eddy SS, Victorio RA, Beerens M, Flaumenhaft R, Deo RC, MacRae CA. PIEZO1 mediates a mechanothrombotic pathway in diabetes. Sci Transl Med. 2022;14(626): eabk1707.
17. Zong B, Yu F, Zhang X, Pang Y, Zhao W, Sun P, Li L. Mechanosensitive Piezo1 channel in physiology and pathophysiology of the central nervous system. Ageing Res Rev. 2023;90: 102026.
18. Yen HC, Oberley TD, Vichitbandha S, Ho YS, St Clair DK. The protective role of manganese superoxide dismutase against adriamycin-induced acute cardiac toxicity in transgenic mice. J Clin Investig. 1996;98(5):1253–60.
19. Chang C, He F, Ao M, Chen J, Yu T, Li W, Li B, Fang M, Yang T. Inhibition of Nur77 expression and translocation by compound B6 reduces ER stress and alleviates cigarette smoke-induced inflammation and injury in bronchial epithelial cells. Front Pharmacol. 2023;14:1200110.
20. Yang M, Abudureyimu M, Wang X, Zhou Y, Zhang Y, Ren J. PHB2 ameliorates Doxorubicin-induced cardiomyopathy through interaction with NDUFV2 and restoration of mitochondrial complex I function. Redox Biol. 2023;65: 102812.

21. Zou R, Tao J, He J, Wang C, Tan S, Xia Y, Chang X, Li R, Wang G, Zhou H, Fan X. PGAM5-mediated PHB2 dephosphorylation contributes to diabetic cardiomyopathy by disrupting mitochondrial quality surveillance. Research. 2022;2022:0001.
22. Tao J, Qiu J, Zheng J, Li R, Chang X, He Q. Phosphoglycerate mutase 5 exacerbates alcoholic cardiomyopathy in male mice by inducing prohibitin-2 dephosphorylation and impairing mitochondrial quality control. Clin Transl Med. 2024;14(8): e1806.
23. Wang J, Pu X, Zhuang H, Guo Z, Wang M, Yang H, Li C, Chang X. Astragaloside IV alleviates septic myocardial injury through DUSP1-Prohibitin 2 mediated mitochondrial quality control and ER-autophagy. J Adv Res. 2024;S2090–1232(24):00471–5.
24. Meng X-W, He C-X, Chen X, Yang X-S, Liu C. The extract of Gnaphalium affine D. Don protects against H2O2-induced apoptosis by targeting PI3K/AKT/GSK-3β signaling pathway in cardiomyocytes. J Ethnopharmacol. 2021;268: 113579.
25. Wang J, Zhu P, Li R, Ren J, Zhang Y, Zhou H. Bax inhibitor 1 preserves mitochondrial homeostasis in acute kidney injury through promoting mitochondrial retention of PHB2. Theranostics. 2020;10(1):384–97.
26. Ren J, Ren B, Fu T, Ma Y, Tan Y, Zhang S, Li Y, Wang Q, Chang X, Tong Y. Pyruvate kinase M2 sustains cardiac mitochondrial integrity in septic cardiomyopathy by regulating PHB2-dependent mitochondrial biogenesis. Int J Med Sci. 2024;21(6):983–93.
27. Wang J, Zhuang H, Jia L, He X, Zheng S, Ji K, Xie K, Ying T, Zhang Y, Li C, Chang X. Nuclear receptor subfamily 4 group A member 1 promotes myocardial ischemia/reperfusion injury through inducing mitochondrial fission factor-mediated mitochondrial fragmentation and inhibiting FUN14 domain containing 1-depedent mitophagy. Int J Biol Sci. 2024;20(11):4458–75.
28. Zou R, Shi W, Chang X, Zhang M, Tan S, Li R, Zhou H, Li Y, Wang G, Lv W, Fan X. The DNA-dependent protein kinase catalytic subunit exacerbates endotoxemia-induced myocardial microvascular injury by disrupting the MOTS-c/JNK pathway and inducing profilin-mediated lamellipodia degradation. Theranostics. 2024;14(4):1561–82.
29. Pu X, Zhang Q, Liu J, Wang Y, Guan X, Wu Q, Liu Z, Liu R, Chang X. Ginsenoside Rb1 ameliorates heart failure through DUSP-1-TMBIM-6-mediated mitochondrial quality control and gut flora interactions. Phytomedicine. 2024;132: 155880.
30. Chang X, Toan S, Li R, Zhou H. Therapeutic strategies in ischemic cardiomyopathy: focus on mitochondrial quality surveillance. EBioMedicine. 2022;84: 104260.
31. Chang X, Li Y, Cai C, Wu F, He J, Zhang Y, Zhong J, Tan Y, Liu R, Zhu H, Zhou H. Mitochondrial quality control mechanisms as molecular targets in diabetic heart. Metabolism. 2022;137: 155313.
32. Chang X, Lochner A, Wang HH, Wang S, Zhu H, Ren J, Zhou H. Coronary microvascular injury in myocardial infarction: perception and knowledge for mitochondrial quality control. Theranostics. 2021;11(14):6766–85.
33. Pang B, Dong G, Pang T, Sun X, Liu X, Nie Y, Chang X. Emerging insights into the pathogenesis and therapeutic strategies for vascular endothelial injury-associated diseases: focus on mitochondrial dysfunction. Angiogenesis. 2024;27(4):623–39.
34. Yu Z, Deng P, Chen Y, Lin D, Liu S, Hong J, Guan P, Chen J, Zhong M-E, Chen J, Chen X, Sun Y, Wang Y, Wang P, Cai Z, Chan JY, Huang Y, Xiao R, Guo Y, Zeng X, Wang W, Zou Y, Yu Q, Lan P, Teh BT, Wu X, Tan J. Pharmacological modulation of RB1 activity mitigates resistance to neoadjuvant chemotherapy in locally advanced rectal cancer. Proc Natl Acad Sci USA. 2024;121(6): e2304619121.
35. Burridge PW, Li YF, Matsa E, Wu H, Ong S-G, Sharma A, Holmström A, Chang AC, Coronado MJ, Ebert AD, Knowles JW, Telli ML, Witteles RM, Blau HM, Bernstein D, Altman RB, Wu JC. Human induced pluripotent stem cell-derived cardiomyocytes recapitulate the predilection of breast cancer patients to doxorubicin-induced cardiotoxicity. Nat Med. 2016;22(5):547–56.
36. Huang H, Christidi E, Shafaattalab S, Davis MK, Tibbits GF, Brunham LR. RARG S427L attenuates the DNA repair response to doxorubicin in induced pluripotent stem cell-derived cardiomyocytes. Stem Cell Rep. 2022;17(4):756–65.
37. Zhao Y, Liu Y, Tao T, Zhang J, Guo W, Deng H, Han M, Mo H, Tong X, Lin S, Yang J, Zhai H, Wang Q, Hu Z, Zhang W, Chen H, Xu G. Gastric mechanosensitive channel Piezo1 regulates ghrelin production and food intake. Nat Metab. 2024;6(3):458–72.
38. Zhou Z, Ma X, Lin Y, Cheng D, Bavi N, Secker GA, Li JV, Janbandhu V, Sutton DL, Scott HS, Yao M, Harvey RP, Harvey NL, Corry B, Zhang Y, Cox CD. MyoD-family inhibitor proteins act as auxiliary subunits of Piezo channels. Science. 2023;381(6659):799–804.
39. Zhuang C, Gould JE, Enninful A, Shao S, Mak M. Biophysical and mechanobiological considerations for T-cell-based immunotherapy. Trends Pharmacol Sci. 2023;44(6):366–78.
40. Su S, Wang J, Wang J, Yu R, Sun L, Zhang Y, Song L, Pu W, Tang Y, Yu Y, Zhou K. Cardioprotective effects of gypenoside XVII against ischemia/reperfusion injury: role of endoplasmic reticulum stress, autophagy, and mitochondrial fusion fission balance. Phytother Res. 2022;36(7):2982–98.
41. Wang Y, Wang J, Zhang J, Wang Y, Wang Y, Kang H, Zhao W, Bai W, Miao N, Wang J. Stiffness sensing via Piezo1 enhances macrophage efferocytosis and promotes the resolution of liver fibrosis. Sci Adv. 2024;10(23): eadj3289.
42. Chen C, Dong X, Zhang W, Chang X, Gao W. Dialogue between mitochondria and endoplasmic reticulum-potential therapeutic targets for age-related cardiovascular diseases. Front Pharmacol. 2024;15:1389202.
43. Chang X, Liu J, Wang Y, Guan X, Liu R. Mitochondrial disorder and treatment of ischemic cardiomyopathy: potential and advantages of Chinese herbal medicine. Biomed Pharmacother. 2023;159: 114171.
44. Aboufares El Alaoui A, Buhl E, Galizia S, Hodge JJL, de Vivo L, Bellesi M. Increased interaction between endoplasmic reticulum and mitochondria following sleep deprivation. BMC Biol. 2023;21(1):1.
45. Wang D, Zhou Y, Hua L, Hu M, Zhu N, Liu Y, Zhou Y. The role of the natural compound naringenin in AMPK-mitochondria modulation and colorectal cancer inhibition. Phytomedicine. 2024;131: 155786.
46. Pan G-P, Liu Y-H, Qi M-X, Guo Y-Q, Shao Z-L, Liu H-T, Qian Y-W, Guo S, Yin Y-L, Li P. Alizarin attenuates oxidative stress-induced mitochondrial damage in vascular dementia rats by promoting TRPM2 ubiquitination and proteasomal degradation via Smurf2. Phytomedicine. 2024;135: 156119.
47. Zhu M-L, Yu Y-N, Song Y-T, Wang C-Y, Miao Z, Chen B-L, Guo S, Shen M-M, Zhang M-X, Zhan H-Q, Yang P-F, Wang Q-Q, Yin Y-L, Li P. Cardioprotective role of A-cycloglycosylated derivative of Rubiadin in diabetic cardiomyopathy in rats. Int Immunopharmacol. 2023;118: 110008.
48. Zhou H, Dai Z, Li J, Wang J, Zhu H, Chang X, Wang Y. TMBIM6 prevents VDAC1 multimerization and improves mitochondrial quality control to reduce sepsis-related myocardial injury. Metabolism. 2023;1(140): 155383.
49. Chang X, Zhou S, Liu J, Wang Y, Guan X, Wu Q, Liu Z, Liu R. Zishenhuoxue decoction-induced myocardial protection against ischemic injury through TMBIM6-VDAC1-mediated regulation of calcium homeostasis and mitochondrial quality surveillance. Phytomedicine. 2024;132: 155331.
50. Zhang X, Zhou H, Chang X. Involvement of mitochondrial dynamics and mitophagy in diabetic endothelial dysfunction and cardiac microvascular injury. Arch Toxicol. 2023;97(12):3023–35.
51. Zhang X, Zhou Y, Chang X, Wu Q, Liu Z, Liu R. Tongyang Huoxue decoction (TYHX) ameliorating hypoxia/reoxygenation-induced disequilibrium of calcium homeostasis via regulating β-tubulin in rabbit sinoatrial node cells. J Ethnopharmacol. 2024;318(Pt B): 117006.
52. Chang X, Li Y, Liu J, Wang Y, Guan X, Wu Q, Zhou Y, Zhang X, Chen Y, Huang Y, Liu R. ß-tubulin contributes to Tongyang Huoxue decoction-induced protection against hypoxia/reoxygenation-induced injury of sinoatrial node cells through SIRT1-mediated regulation of mitochondrial quality surveillance. Phytomedicine. 2023;108: 154502.
53. Chang X, Ismail NI, Rahman A, Xu D, Chan RWY, Ong SG, Ong SB. Long COVID-19 and the heart: is cardiac mitochondria the missing link? Antioxid Redox Signal. 2023;38(7–9):599–618.
54. Yang K, Zhang P, Li J, Zhang G, Chang X. Potential of natural drug modulation of endoplasmic reticulum stress in the treatment of myocardial injury. J Pharm Anal. 2024;14(11): 101034.
55. Wu Y, Chen Q, Wen B, Wu N, He B, Chen J. Berberine reduces Aβ42 deposition and Tau hyperphosphorylation via ameliorating endoplasmic reticulum stress. Front Pharmacol. 2021;12: 640758.
56. Zhao B, Wei D, Long Q, Chen Q, Wang F, Chen L, Li Z, Li T, Ma T, Liu W, Wang L, Yang C, Zhang X, Wang P, Zhang Z. Altered synaptic currents, mitophagy, mitochondrial dynamics in Alzheimer's disease models and therapeutic potential of Dengzhan Shengmai capsules intervention. J Pharm Anal. 2024;14(3):348–70.
57. Zhang C, Chang X, Zhao D, He Y, Dong G, Gao L. Mitochondria and myocardial ischemia/reperfusion injury: effects of Chinese herbal medicine and the underlying mechanisms. J Pharm Anal. 2025;15(2): 101051.

58. Zhu L, Zhang Q, Meng F, Li M, Liang Q, Zhang F. Narrow-pore engineering of vinylene-linked covalent organic frameworks with weak interaction-triggered multiple responses. Angew Chem Int Ed Engl. 2023;62(42): e202309125.
59. Zou L, Liu X, Li J, Li W, Zhang L, Fu C, Zhang J, Gu Z. Redox-sensitive carrier-free nanoparticles self-assembled by disulfide-linked paclitaxel-tetramethylpyrazine conjugate for combination cancer chemotherapy. Theranostics. 2021;11(9):4171–86.
60. Zhou Y, Wu R, Wang X, Jiang Y, Xu W, Shao Y, Yue C, Shi W, Jin H, Ge T, Bao X, Lu C. Activation of UQCRC2-dependent mitophagy by tetramethylpyrazine inhibits MLKL-mediated hepatocyte necroptosis in alcoholic liver disease. Free Radical Biol Med. 2022;179:301–16.
61. Zhu Z, Li J, Song Z, Li T, Li Z, Gong X. Tetramethylpyrazine attenuates renal tubular epithelial cell ferroptosis in contrast-induced nephropathy by inhibiting transferrin receptor and intracellular reactive oxygen species. Clin Sci. 2024;138(5):235–49.

Publisher's Note

Springer Nature remains neutral with regard to jurisdictional claims in published maps and institutional affiliations.